

Structure, fragmentation patterns, and magnetic properties of small nickel oxide clusters

R. H. Aguilera-del-Toro,^{1,2} F. Aguilera-Granja,¹ L.C. Balbás,^{2,*} and A. Vega²

¹*Instituto de Física, Universidad Autónoma de San Luis Potosí, San Luis Potosí, México*

²*Departamento de Física Teórica, Atómica y Óptica, Universidad de Valladolid, Spain*

(Dated: June 27, 2016)

Abstract

We report a comprehensive theoretical study of the structural and electronic properties of neutral and charged nickel oxide clusters, $\text{Ni}_n\text{O}_m^{0/\pm}$ ($n=3-8$ and $m=1-10$), in the context of recent experiments of Photodissociation and Ion Mobility Mass Spectrometry. By means of density functional theoretic calculations in the generalized gradient approximation for exchange and correlation, we determined the putative ground states as well as the low-energy structural- and spin- isomers which were then used to explore the favourable fragmentation channels of the nickel oxide cationic clusters, and the resulting most abundant products, in good qualitative agreement with Photodissociation measurements. Apart from stoichiometries different from those of nickel oxide macroscopic counterparts, we found a tendency to form compact Ni subclusters, with reentrance of low-coordinated structures close to the equiatomic Ni-O concentration, taking the form of alternating Ni-O rings in the smaller sizes, in good qualitative agreement with Ion Mobility Mass Spectrometry measurements. This structural pattern is manifested in a drop of the total spin magnetic moment close to the equiatomic concentration due to the formation of antiparallel magnetic couplings. Although antiparallel couplings are found in a more or less extent in most clusters, specially in the oxygen rich phase, we identified certain clusters of special interest in the context of magnetic grains because of their large total magnetic moment and abundance. This fact demonstrates that the unavoidable oxidation in environmental conditions does not necessarily quench the magnetic moment, but can even enhance it in some cases by promoting parallel magnetic couplings.

PACS numbers: 75.75+a; 36.40Cg; 75.30.Pd; 75.50.-y

Keywords: DFT calculations, structure, electronic, and energetic properties, transition-metal oxide clusters

I. INTRODUCTION

With the continuous trend of designing nanostructures to achieve unprecedented goals beyond the capabilities of macroscopic devices, transition-metal (TM) oxide nanoparticles (NPs) are becoming a desired target in many areas like nanomagnetism, nanocatalysis and nanomedicine. TM oxide NPs exhibit a variety of relevant properties in those contexts, depending on the TM component and stoichiometry. Besides, there is an increasing interest in replacing hazardous, costly or scarce materials (commonly classified as critical), and TM oxide NPs are good candidates also in this context. To give just a few concrete examples, Ti oxide NPs are among the most abundant with a global production of about 3000 tons per year^{1,2}. They are commonly used in food products and against microorganisms^{3,4}, and more particularly as growth inhibitors of oral bacteria⁵. NPs of magnetite (Fe_3O_4) are widely used as contrast agents in clinical magnetic resonance imaging, due to their magnetic properties, low toxicity and known pathways of metabolism⁶. Co oxide NPs are useful in storage media and biomedical sensing⁷⁻⁹. Ni oxide NPs have been used in chemical sensors, and more particularly to construct a carbon composite electrode for the determination of paracetamol and some neurotransmitters¹⁰. In fact, Ni oxide compounds are widely used in anodes in electrochemical cells¹¹, in chemical sensors¹² and in catalysts of reactions such as CO oxidation^{13,14} or water splitting^{15,16}. Therefore, the potential of Ni oxide NPs in those contexts must be enormous.

Although the Ni oxide macroscopic compounds are well known and, for instance, the atomic structure and stable stoichiometries are well characterized, detailed information about fundamental properties of Ni oxide NPs is still scarce. The geometrical structure is, probably, the most elusive fundamental property of free-standing NPs, due to the fact that well stabilised and accurate spectroscopic or crystallographic techniques (see for example Mordy and coworkers¹⁷), used to characterize extended systems, are not useful for non-supported NPs like clusters produced by laser vaporization of metal rods in a pulsed nozzle cluster source. Besides, in the cluster regime, the structural and electronic properties are often unique for a specific cluster size. The stoichiometry of the most abundant (with highest relative stability) individuals for a given size of the NP may not correspond to the natural stoichiometries of one of the macroscopic counterparts¹⁸. Another fundamental property is the electronic structure, which is directly connected to the geometrical

structure of the NP, as the electron density is slave of the ionic potential. The geometrical and electronic structures of the NP determine the magnetic properties and reactivity, which are the key ingredients for designing efficient NPs for the applications described in the first paragraph. Photodissociation experiments of mass-selected clusters, combined with density functional theory (DFT) calculations allow to investigate their growth and stability patterns, as well as to characterize their putative ground state from both the structural and electronic points of view. Another experimental technique that can be used, when combined with DFT calculations, for the determination of the putative cluster structure, is the Ion Mobility Mass Spectrometry (IMMS).

The favorable stoichiometries of Ni_nO_m^+ cationic clusters **produced by laser vaporization of metal rods in a pulsed nozzle source** have been recently determined by means of **time-of-flight mass spectrometry**. It was obtained from these mass spectra that the prominent stoichiometry of Ni_nO_m^+ is $m = n - 1$ in competition with $n = m$. **The cluster cations were mass selected and photodissociated by multiple photons of 355 nm (3.49 eV). The resulting Ni_nO_m^+ fragments reveal a loss of O_2 and a preference of metal-rich fragments with stoichiometries of $\text{Ni}_x\text{O}_{x-1}$, being the Ni_2O^+ fragment produced from many parent ions.** The structures of Ni_nO_m^+ cationic clusters of certain stoichiometries have been also investigated by IMMS very recently¹⁹ (they also study CO-adsorption reactivities). They have complemented the experiments with calculations within the DFT as implemented in Gaussian code. For Ni_xO_x and $\text{Ni}_x\text{O}_{x-1}$ they propose an assignment of the involved geometries, which are those for which their calculated collision cross section fitted the experimental measurement. However, in many cases those proposed geometries are highly excited states, with energy differences of about 1eV or more with respect to their putative ground state. It is hardly probable that those metastable states are accessible at the experimental conditions, so that the authors themselves indicate the need of more accurate calculations.

The aim of the present work is to characterize the fundamental properties of small Ni oxide clusters, in both the neutral and charged states, by means of systematic DFT calculations in the generalized gradient approximation (GGA) for exchange and correlation, and an exhaustive comparison with the photodissociation measurements of Dibble *at al.*¹⁸. We calculate the putative ground states and the more favorable fragmentation channels. We calculate the spin-polarized electronic structure in order to analyze the magnetic properties

as a function of relative oxygen concentration and charge states. We explore the isomeric map, from both the structural and spin configurations, in order to find metastable Ni oxide NPs that could be also of interest, as well as to compare with the isomeric map obtained by Ohshimo *et al.*¹⁹ for the cationic clusters using a different DFT approach. Thus, the results of the present work complement the two previous experimental investigations with the final goal of giving a step forward in the knowledge of the fundamental properties of small Ni oxide clusters.

The paper is organized as follows. In Sec. II, we describe the theoretical and computational approaches. The results are discussed in different subsections of section III: in subsection III A are discussed the ionic structures and energetics; in subsection III B the favorable fragmentation channels are studied by comparing the minimum energy needed for the separation of different fragments; in subsection III C are studied the magnetic properties. The conclusions are summarized in section IV at the end.

II. THEORETICAL APPROACH AND COMPUTATIONAL DETAILS

We performed fully self-consistent DFT calculations using the SIESTA code²⁰, which solves the spin-polarized Kohn-Sham equations within the pseudopotential approach. For the exchange and correlation potential we used the Perdew-Burke-Ernzerhof form of the generalized gradient approximation (GGA).²¹ We employed norm-conserving scalar relativistic pseudopotentials²² in their fully nonlocal form²³, generated from the atomic valence configuration $3d^8 4s^2$ for Ni (with core radii 2.00, 2.32 and 2.44 a.u. for s , p and d orbitals respectively), and $2s^2 2p^4$ for O (with core radii 1.14 a.u. for s , p and d orbitals) Non-linear partial core corrections²⁴, which are known to be important for transition metal pseudopotential, are included for Ni at the core radius 0.7 Å.

Valence states were described using double- ζ basis sets for O and Co, with maximum cutoff radii radius 4.931 Å ($2p$) and 7.998 Å ($3d, 4s$), respectively. A $4p$ polarization orbital was also considered for Ni, with cutoff radius 7.998 Å.

The energy cutoff used to define the real-space grid for numerical calculations involving the electron density was 250 Ry. The Fermi distribution function that enters in the calculation of the density matrix was smoothed with an electronic temperature of 15meV. We used an energy criterium of 10^{-4} eV for converging the electronic part.

In the calculations, the individual clusters were placed in a cubic supercell of $20 \times 20 \times 20 \text{ \AA}^3$, a size large enough to neglect the interaction between the cluster and its replicas in neighboring cells. It was considered only the Γ point ($k = 0$) when integrating over the Brillouin zone, as usual for finite systems.

The equilibrium geometries resulted from an unconstrained conjugate-gradient structural relaxation using the DFT forces. Initial geometries were built by considering different arrangements of the Ni and O atoms without privileging those formed from given Ni subclusters. Thus, an exhaustive sampling of possible geometries was tested, including those in which the possibly strong Ni-O bonding prevents the nucleation of compact Ni subclusters. Structures were relaxed without any symmetry constraint until interatomic forces were smaller than $0.003\text{eV}/\text{\AA}$. In all cases, different spin isomers were checked in order to ensure the correct ground state. For that search of spin isomers, the criterium for maximum interatomic forces was further reduced to $0.001\text{eV}/\text{\AA}$.

For selected clusters, we performed a benchmark against results obtained using the VASP code^{25,26} with the same PBE functional. VASP employs a plane-waves basis set instead of numerical pseudoatomic orbitals, and the core interactions are treated by means of the projector-augmented wave (PAW) approach instead of pseudopotentials. In all cases the agreement with our SIESTA setup was fine.

III. RESULTS AND DISCUSSION

A. Geometrical configurations and electronic properties

We describe here the geometrical properties of the investigated $\text{Ni}_n\text{O}_m^{0/\pm}$ ($n = 3-8$ and $m = 1-10$) clusters. Before going into the structural details for each n series, we summarize those trends and growth patterns that are common to all or most of them. We focus on the cationic clusters, since it is the charge state of the clusters present in the experimental analysis. In Figs. 1 to 6 are depicted the putative ground state and first two low-energy isomers of the cationic clusters. The ground state of their neutral and anionic counterparts, when not the same, corresponds to one of the two lowest-energy isomers, and it can be identified in Tables I-XII of the **appendix**, where inter-atomic distances, binding energies and total spin-magnetic moment are also reported.

In the initial stages of oxidation, for all n , a compact Ni_n subcluster is formed, on which oxygen atoms start to bond preferentially in three-fold hollow sites, and then in bridge sites. This Ni_n motif is robust until $m \approx n$ and, up to this point, the growth pattern proceeds simply by capping Ni_n with O avoiding direct O-O bonding (oxygen atoms tend to distribute uniformly on the cluster). When $m \approx n$, a structural change takes place. The structure opens and the cluster adopts a low-coordinated arrangement, with a weakening of the Ni-Ni bonding manifested in an increase of Ni-Ni inter-atomic distance and a lowering of the Ni-O one, as seen in the Figure 7. The Ni-Ni coordination also reduces in general at this transition (Fig. 8). This is particularly notorious for clusters with $n < 6$, for which two-dimensional ring-like structures are formed at the stoichiometric or equiatomic oxidation rate ($m = n$). Those ring-like structures have, in general, a high relative stability in agreement with experiments, as well as exceptional magnetic properties (to be discussed in section III C). For $n \geq 6$, this opening of the geometrical structure as m approaches n is less dramatic (planar ring-like structures are not formed) though it is still recognizable (see 6.5-I, 7.5-I, 8.8-I). After this reentrance of low-coordinated arrangements at $m \approx n$, the structure becomes again relatively compact at higher oxidation rates. This is again reflected in the average inter-atomic distances (Fig. 7) and coordination (Fig. 8). However, at higher oxidation rates, the structures become more complex. Although in most cases, similar Ni_n motifs as those formed for low oxidation rates can be still identified, other motifs based on the stable ring structures of smaller stoichiometric clusters can be also identified in some cases. The distribution of the Ni-O inter-atomic distances becomes narrow as the cluster size increases, regardless the charge state. As we will see, the reentrance of low coordinated structures close to the stoichiometric oxidation rate also correlates with the magnetic properties. Besides, the maximal value of the Ni-Ni inter-atomic distance corresponds with a minimal value in the magnetic moment, the only exception is observed for Ni_4O_4 . The geometries of the neutral and anionic Ni oxide clusters are, in most cases, similar to those of their cationic counterparts; when different, a more open structure is formed as a general rule. The favorable site for O (hollow or bridge) changes, in some cases, with the charge state. Those cases can be identified in Fig. 8 through different Ni-O average inter-atomic distances reflecting a rearrangement of one or more oxygen atoms depending on the charge state. Note that this may happen even if the Ni subcluster is preserved. Changes in the Ni subcluster upon an electron deficit or excess are manifested in different

Ni-Ni average interatomic distances and can be easily identified also in Fig. 8. Details of the corresponding ground states are collected in the tables of the SI. Exceptions to the above rules are only Ni_6O and Ni_6O_5 , with different Ni subcluster in different charge states but with the same average Ni-Ni and Ni-O distance.

The binding energy per atom of neutral and charged clusters, as well as the second total energy difference is plotted, as a function of the oxygen content m , in Figure 9. These magnitudes are defined as follows:

$$E_b^0(n, m) = [n \times E(\text{Ni}) + m \times E(\text{O}) - E(n, m)^0]/(n + m)$$

$$E_b^\pm(n, m) = [E(\text{Ni})^\pm + (n - 1) \times E(\text{Ni}) + m \times E(\text{O}) - E(n, m)^\pm]/(n + m)$$

and

$$\Delta_2(n, m) = E(n, m - 1)^{0/\pm} + E(n, m + 1)^{0/\pm} - 2 \times E(n, m)^{0/\pm}$$

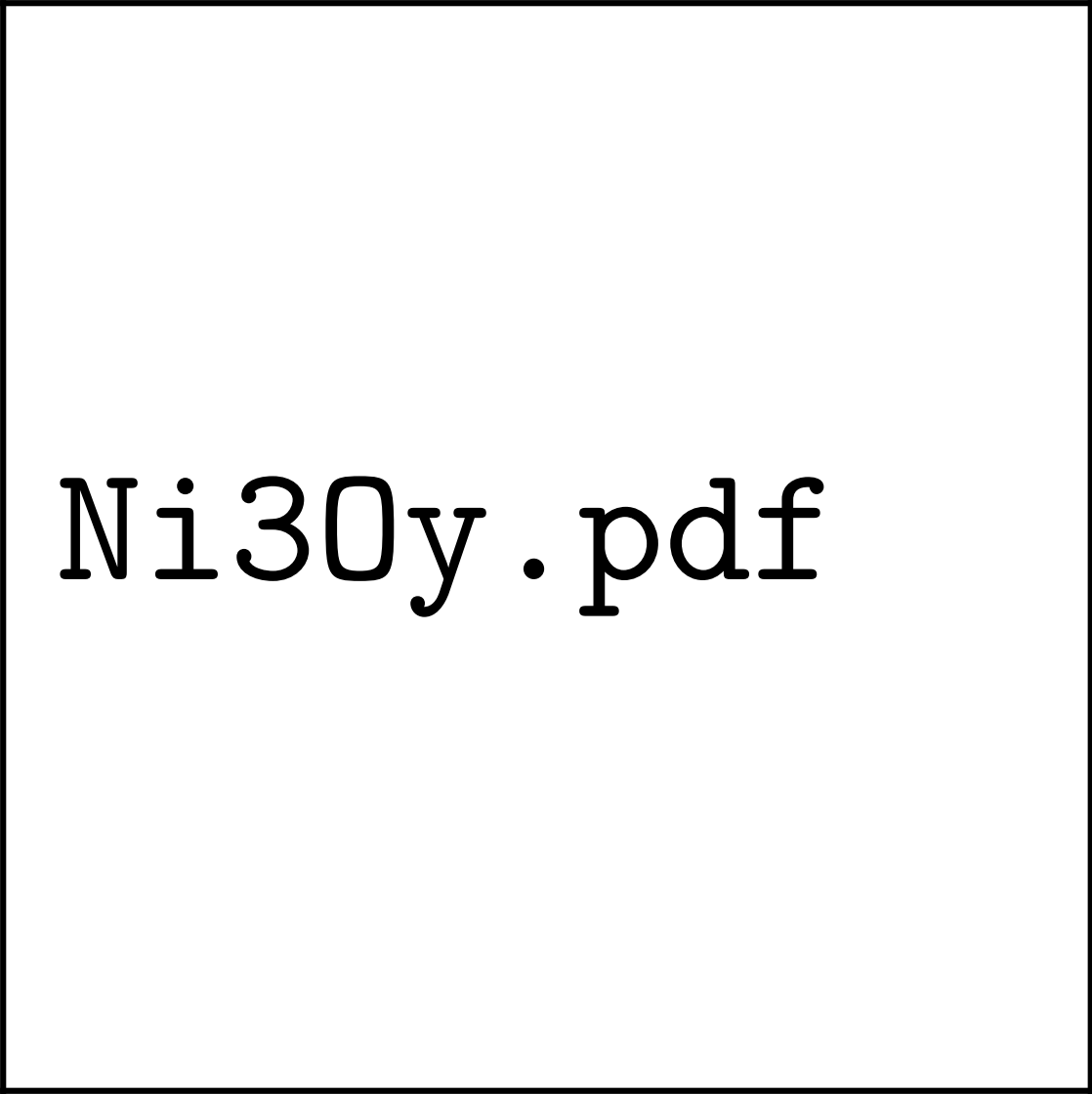
where $E(n, m)^{0/\pm}$ are the total energy of the $\text{Ni}_n\text{O}_m^{0/\pm}$ clusters. For a given n , the values $\Delta_2(n, m)$ as a function of m will show a prominent positive peak at those m values whose corresponding (n, m) clusters are more stable than their $(n, m - 1)$ and $(n, m + 1)$ neighbors against the addition or subtraction of one oxygen atom.

It is worth noticing that, in general, the picks in the second energy difference correspond to clusters that are formed by a fundamental building block made of two Ni and one oxygen atoms in an isosceles triangular arrangement, being the Ni-Ni the largest distance in the block. The fundamental block formed by Ni_2O is also present in larger unities with high stability, like the rhombus Ni_2O_2 and the Ni_3O_3 ring, that can be clearly identified in the putative ground states $(n, m - I)$ as illustrated in the Figures 1-6. Some deviations in this trend are observed in the anionic clusters particularly for Ni_5 and Ni_6 .

In the remaining of this section we describe the structural details for each n series. As we will see, the highest relative stability deduced from $\Delta_2(n, m)$ corresponds indeed to two-dimensional ring structures, or to structures in which rings of lower size clusters can be identified.

1. $[\text{Ni}_3\text{O}_m]^+$, $m = 1-6$

Most clusters in this series have a triangular core of nickel atoms, not only the putative ground states but also the lowest isomers, an exception being the linear 3.3-II. In poor oxygen clusters ($m \leq 2$), O atoms bind on hollow sites, while bridge positions are more



Ni₃O_y.pdf

FIG. 1: (Color online) Putative ground state and first two low-energy isomers of $[\text{Ni}_3\text{O}_m]^+$ with $m = 1-6$. The notation is 3. m -Label, with Label in roman letters in decreasing order of stability for each (3, m).

favourable in rich oxygen clusters ($m \geq 3$). Certain isomers have quite singular structural properties, only present in this series; these are: 3.1-III, with the oxygen atom bonded on top position; 3.3-III, the only geometry with O atoms bonded in all kind of sites (hollow, bridge and top positions); 3.4-I, with a molecular oxygen bonded on bridge; 3.4-III, with two oxygen atoms molecularly bonded on top; 3.5-II and 3.6-II, with three atoms on top; and 3.6-I, with three oxygen atoms molecularly bonded to the nickel subcluster. The cluster 3.3-I

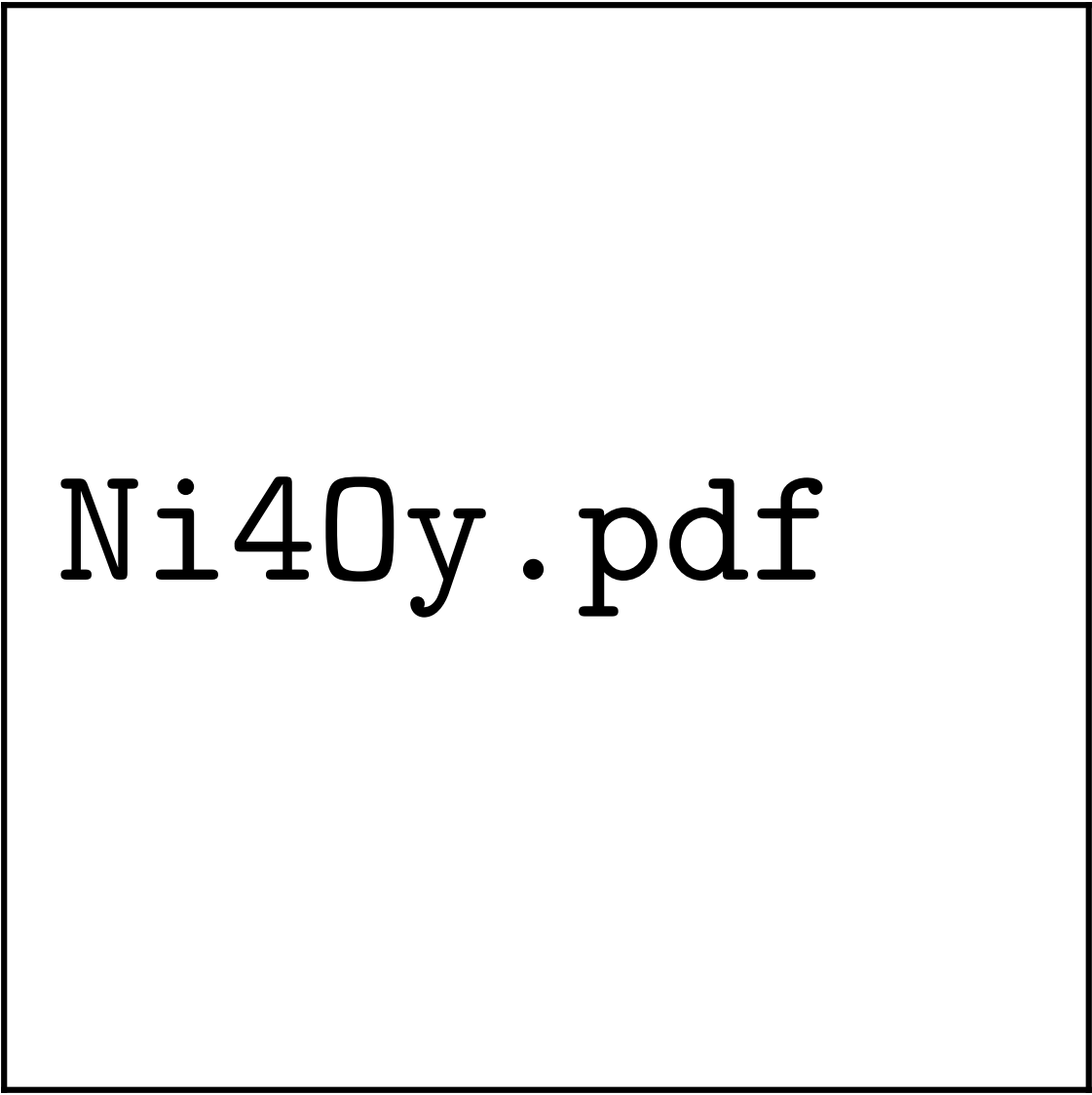
has a planar ring-like structure, it has the largest binding energy per atom and the highest relative stability, manifested in the peak in the second energy difference, independently of the charge state, being the most stable one for this series. Furthermore, the average Ni-O inter-atomic distance (regardless of the charge state) has a minimal value. As we will see later, this is consistent with its abundance, as experimentally observed. This ring structure can be also identified in 3.4-I and 3.5-I, where it is capped by one and two additional oxygen atoms, respectively.

2. $[Ni_4O_m]^+$, $m = 1-7$

Most clusters have a tetrahedral Ni_4 core. The exception is 4.4.I with a planar ring-like structure (again for all charge states). This cluster has the largest binding energy per atom for the neutral and anionic states, while for the cationic one it has the same energy per atom as 4.5.I. On the other hand, the average Ni-O inter atomic distance for this cluster has a minimal value, while the Ni-Ni one has a maximum value only for the cationic cluster. Due to its relevance in the context of the experiments, we devote part of section III.C to a detailed discussion of the magnetic properties of $Ni_4O_4^{0/+}$. Planar structures are also found in certain low-energy isomers like 4.1-III and 4.2-III, both having the oxygen atoms bonded in bridge sites. 4.3-III is a Ni_3O_3 ring capped with a nickel atom; 4.5-I, 4.5-II, 4.6-II and 4.6-III can be also described as oxygen-capped ring-like structures.

3. $[Ni_5O_m]^+$, $m = 1-8$

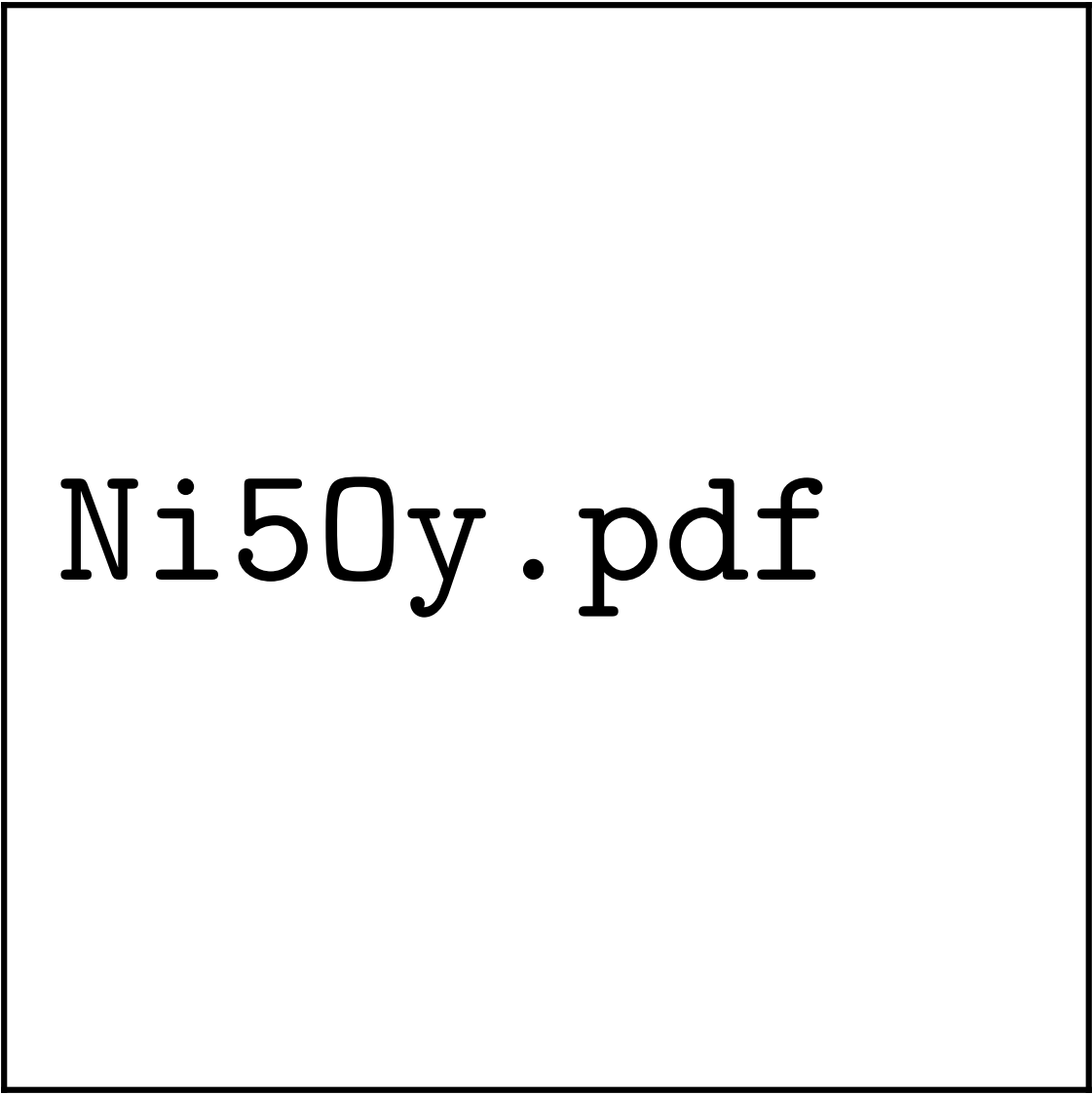
Clusters with low oxygen content have an hexahedron-like core of nickel atoms. The cluster 5.4-I is a pyramid-like one, formed by two Ni_3O_3 rings sharing atoms. It has the largest relative stability, as reflected in the second energy difference (Fig. 9). Thus, the structure starts to open at this oxygen content and, with one just more O atom, 5.5-I already has a planar ring arrangement. This is the biggest planar Ni oxide cluster among all investigated ones. Unlike in the previous series, no peak appears in the second energy difference for this structure, but like in previous series, the average Ni-O inter-atomic distance has a minimal value (maximum for Ni-Ni inter-atomic distance) regardless the charge state. In fact, a transition from two dimensional structures to three-dimensional ones takes place for stoi-



Ni₄O_y.pdf

FIG. 2: (Color online) Putative ground state and first two low-energy isomers of $[\text{Ni}_4\text{O}_m]^+$ with $m = 1-7$. The notation is 4. m -Label, with Label in roman letters in decreasing order of stability for each $(4, m)$.

stoichiometric Ni oxide clusters at this particular size, in agreement with IMMS experiments¹⁹. In clusters 5.6-I, 5.7-I, 5.8-I, a Ni_4O_4 motif can be identified, and a Ni_3O_3 motif in 5.4-I and 5.7-I.



Ni5Oy . pdf

FIG. 3: (Color online) Putative ground state and first two low-energy isomers of $[\text{Ni}_5\text{O}_m]^+$ with $m = 1-8$. The notation is 5. m -Label, with Label in roman letters in decreasing order of stability for each (5, m).

4. $[\text{Ni}_6\text{O}_m]^+$, $m = 1-9$

Almost all structures have an octahedral-like core of nickel atoms. Exceptions are 6.1-I with a capped hexahedral nickel core, which can be seen as the structure of 5.1-I with an additional Ni atom on a hollow site, and 6.5-I formed by a Ni_4O_4 ring capped with a Ni_2O . This last one is the open structure close to the stoichiometric oxidation rate for this series.

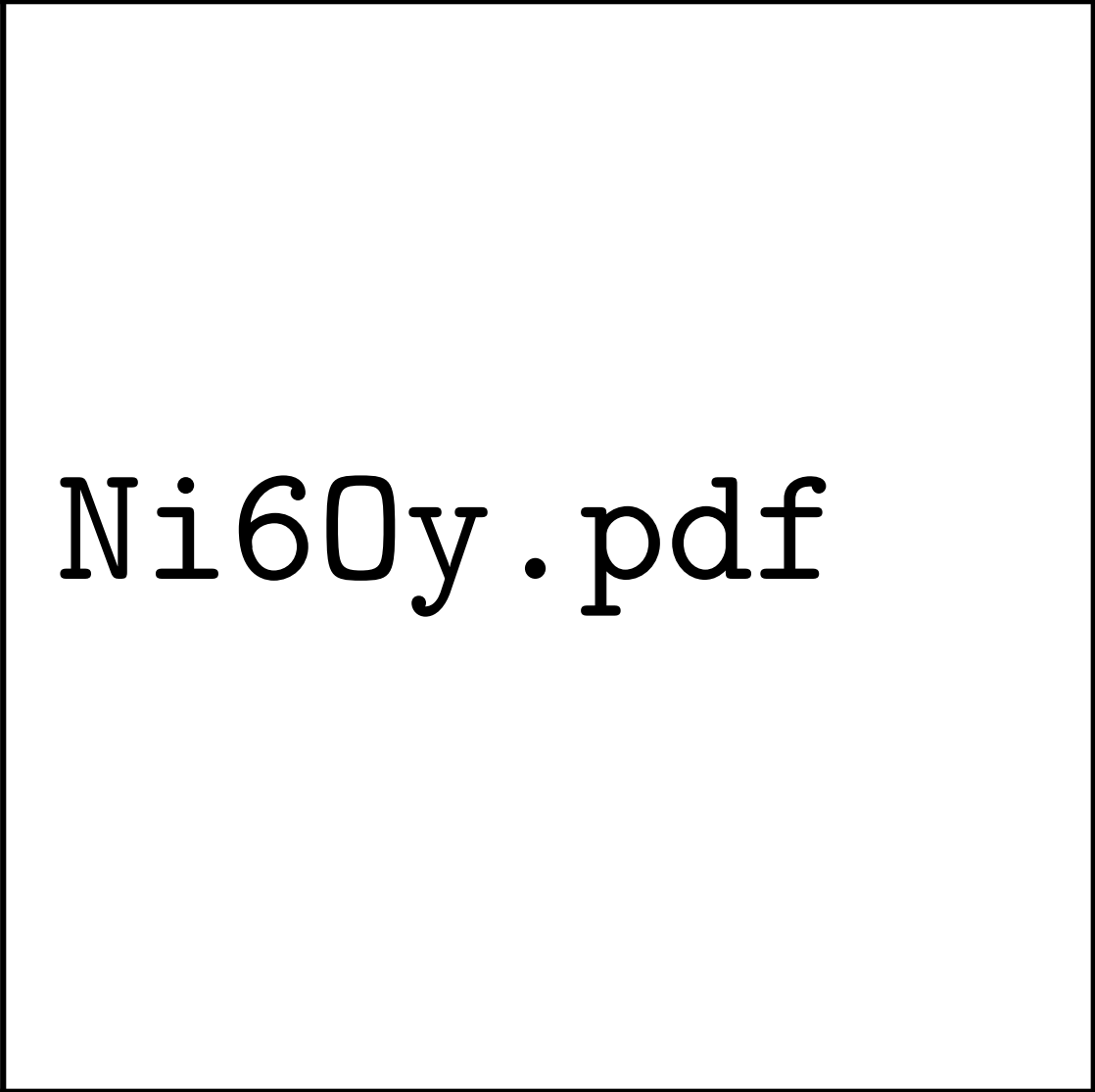
Perfectly planar ring structures are no longer the putative ground state at the stoichiometric rate, but they exist as a low-lying isomer (6.6-III). The stoichiometric ground state, 6.6-I, is formed by two Ni_3O_3 rings one above the other; it has a stability peak in the second energy difference (Fig. 9) and the largest binding energy per atom. This arrangement has a maximum value for the average Ni-Ni inter-atomic distance in the cationic and anionic states. Another particularly stable cluster, in both the cationic and neutral states, is 6.4-I, which leads to the highest peak in the second difference energy. Its structure is an octahedral core of nickel atoms with the oxygen atoms on hollow positions. This structure, of high symmetry (T_d), can also be seen as four interpenetrated Ni_3O_3 rings (located at the shared faces). In clusters 6.3-I, 6.4-I, 6.6-I, a Ni_3O_3 ring motif can be identified.

5. $[\text{Ni}_7\text{O}_m]^+$, $m = 1-10$

The ground state structures of this series have a capped octahedral-like nickel core. The only exception is 7.5-I, which is formed by a Ni_4O_4 ring capped with a Ni_3O_1 subcluster. This is the open structure of this series close to the equiatomic oxidation rate and it has the largest relative stability. No planar structure appears even among the low-energy isomers, but Ni_3O_3 rings can be identified in the surfaces of 7.3-I, 7.4-I, 7.5-I, 7.6-I and 7.8-I, and Ni_4O_4 rings in 7.5-I, 7.6-I, 7.7-I and 7.9-I. Those clusters minimize their energy by using Ni_3O_3 and Ni_4O_4 rings as building blocks. The average Ni-Ni inter atomic distance increases with the number of oxygens atoms, except for the anionic cluster Ni_7O_8 . The Ni-O average inter atomic distances enter in a narrow window of 1.84-1.94 Å. In this series for low O content, the second energy difference display an even-odd effect.

6. $[\text{Ni}_8\text{O}_m]^+$, $m = 1-10$

Almost all ground states have a core of nickel atoms, being a bicapped octahedron for $m = 1, 2, 3$ and 10. Clusters with $m = 4, 5$ and 6 are tower-like, while those with $m = 8$ and 9 are amorphous. Like in other series, rings can be identified in some clusters. 8.5-I has a Ni_4O_4 ring capped with a Ni_4O sub-cluster, being the one with the highest relative stability (the largest pick in the second energy difference); 8.3-I is a Ni_3O_3 ring capped with a Ni_5 sub-cluster; 8.4-I is a Ni_4O_4 ring capped with a Ni_4 sub-cluster; 8.8-I is an open structure



Ni6Oy.pdf

FIG. 4: (Color online) Putative ground state and first two low-energy isomers of $[\text{Ni}_6\text{O}_m]^+$ with $m = 1-9$. The notation is 6. m -Label, with Label in roman letters in decreasing order of stability for each $(6, m)$.

formed by two Ni_3O_3 rings. It is nearly a hollow cage. In 8.9-I, five nickel atoms form a core and the other three are separated. The average Ni-Ni inter atomic distance increases with the number of O atoms, rises, and the Ni-O average inter-atomic distances also enter in a narrow window of 1.84-1.94 Å.

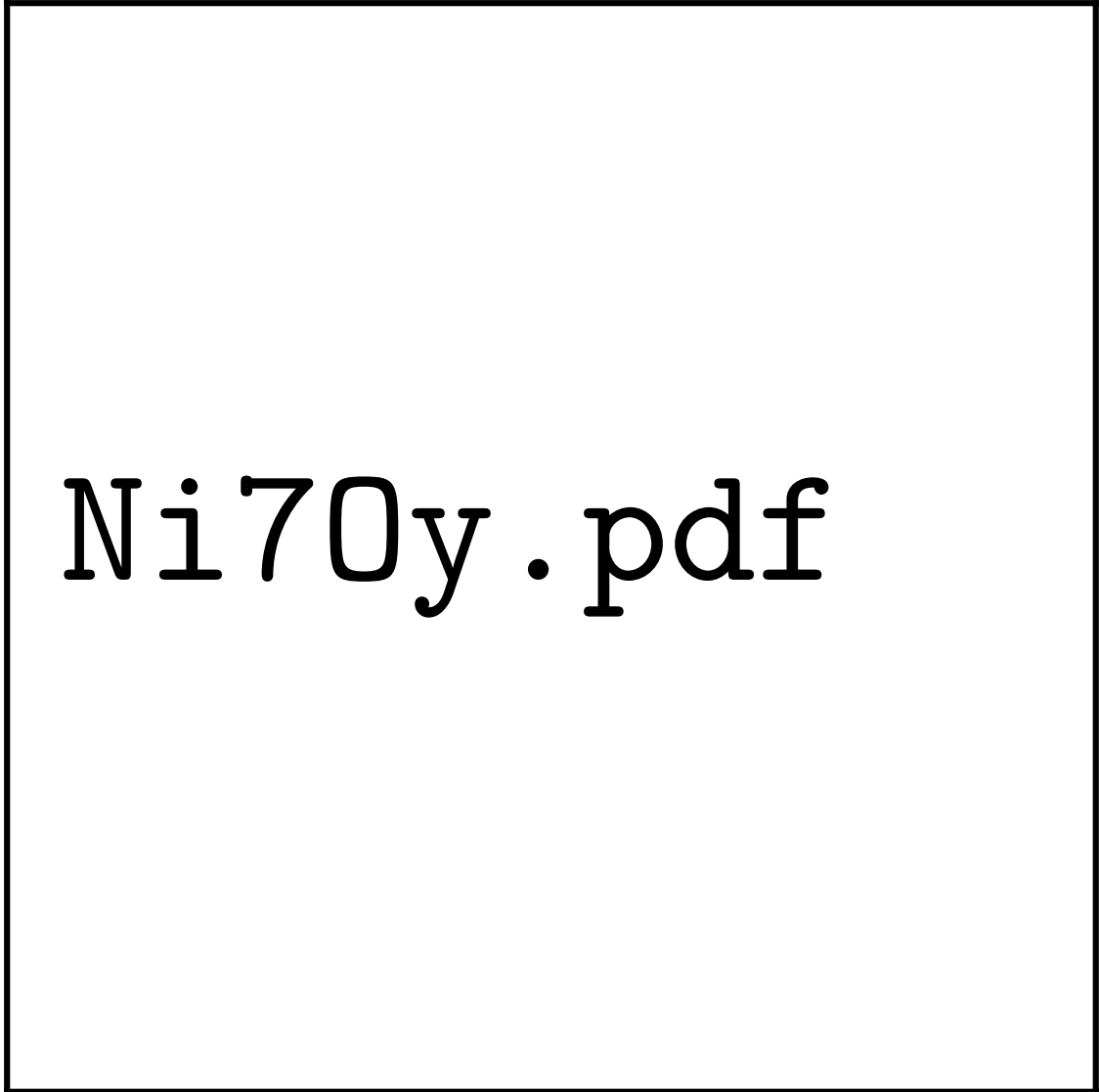
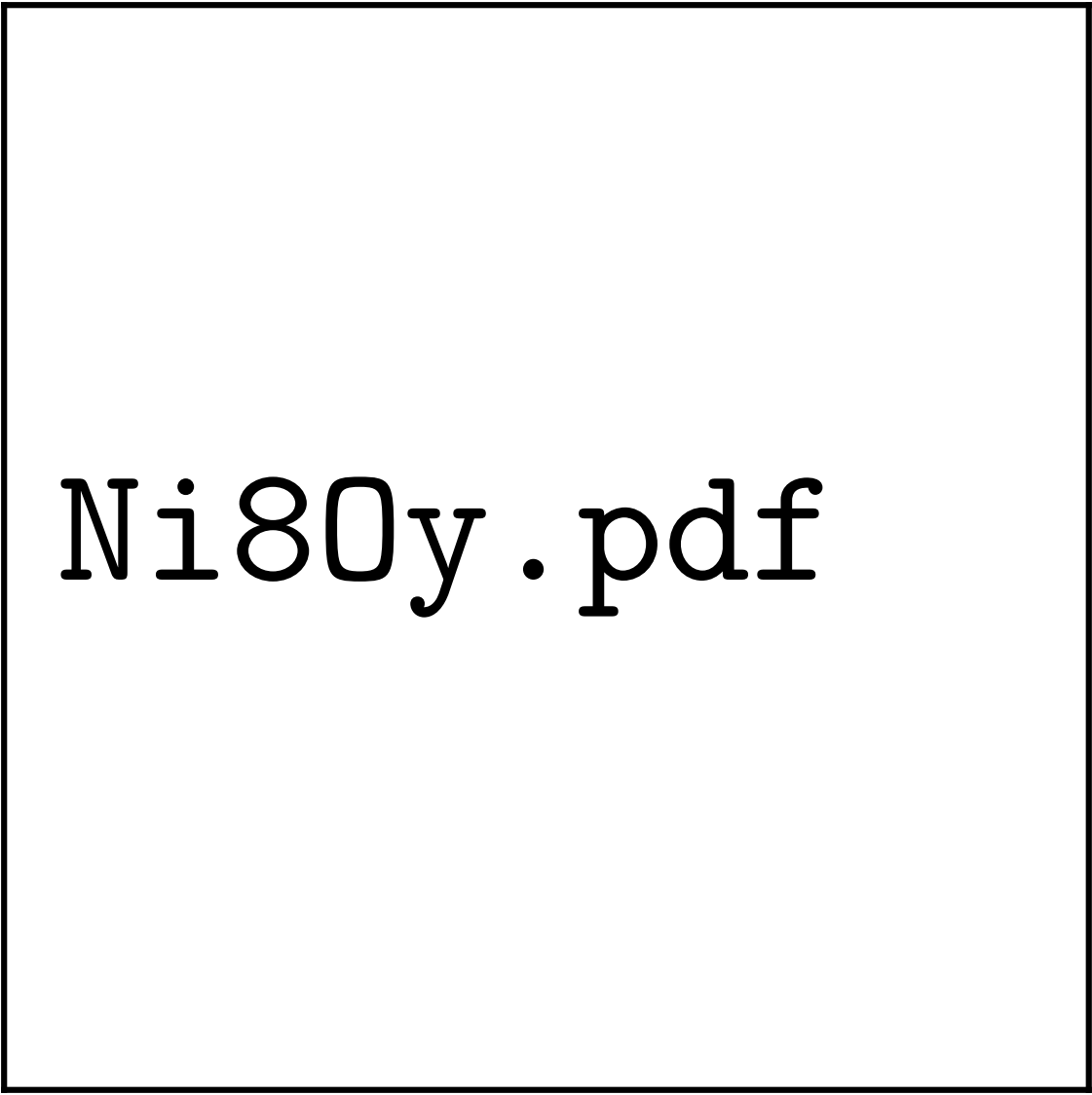


FIG. 5: (Color online) Putative ground state and first two low-energy isomers of $[\text{Ni}_7\text{O}_m]^+$ with $m = 1-10$. The notation is $7.m$ -Label, with Label in roman letters in decreasing order of stability for each $(7, m)$.

B. Fragmentation channels of cationic clusters

The photo-dissociation of mass selected Ni_nO_m^+ cations (denoted as $n.m$ through this paper) is produced experimentally by multiple absorption of photons of 355 nm (3.49 eV)¹⁸. Multiple photons are needed to broke the bond energy of the nickel oxide clusters because, according to our calculations shown in Figure 8, the binding energy per particle is in the



Ni80y . pdf

FIG. 6: (Color online) Putative ground state and first two low-energy isomers of $[\text{Ni}_8\text{O}_m]^+$ with $m = 1-10$. The notation is $8.m\text{-Label}$, with Label in roman letters in decreasing order of stability for each $(8, m)$.

range $\sim 3-4$ eV. A comprehensive list of the photo-fragments produced by several mass selected clusters cations after multiple photon absorption is presented in Table 2 of the work of Duncan and coworkers^{18,28}. As discussed by these authors, the mechanism of fragmentation can be i) of parallel type, with the same parent cluster leading to two or more different fragments, ii) sequential, with a chain of parent-daughter fragments, or iii) a combination of i) and ii). Varying the laser power allows, in principle, distinguish between the i) and ii)



Adistancias-2.1

FIG. 7: (Color online) Ni-Ni (left panels) and Ni-O (right panels) average distance for $\text{Ni}_n\text{O}_m^{0/\pm}$ clusters as a function of the number of oxygen atoms (m).

dissociation processes, but the experimental studies¹⁸, which are consistent with mechanism i), cannot rule out with absolute certainty the sequential fragmentation scheme ii).

From the experimental fragmentation data no direct information about the structure of the precursor cation can be obtained because extensive reorganization of the structures may occurs before fragmentation. In this section we will compare the experimental fragments with those resulting from our total energy calculations and taken into account both, the parallel and sequential mechanisms. For a given step, we first subtract the calculated energies of the

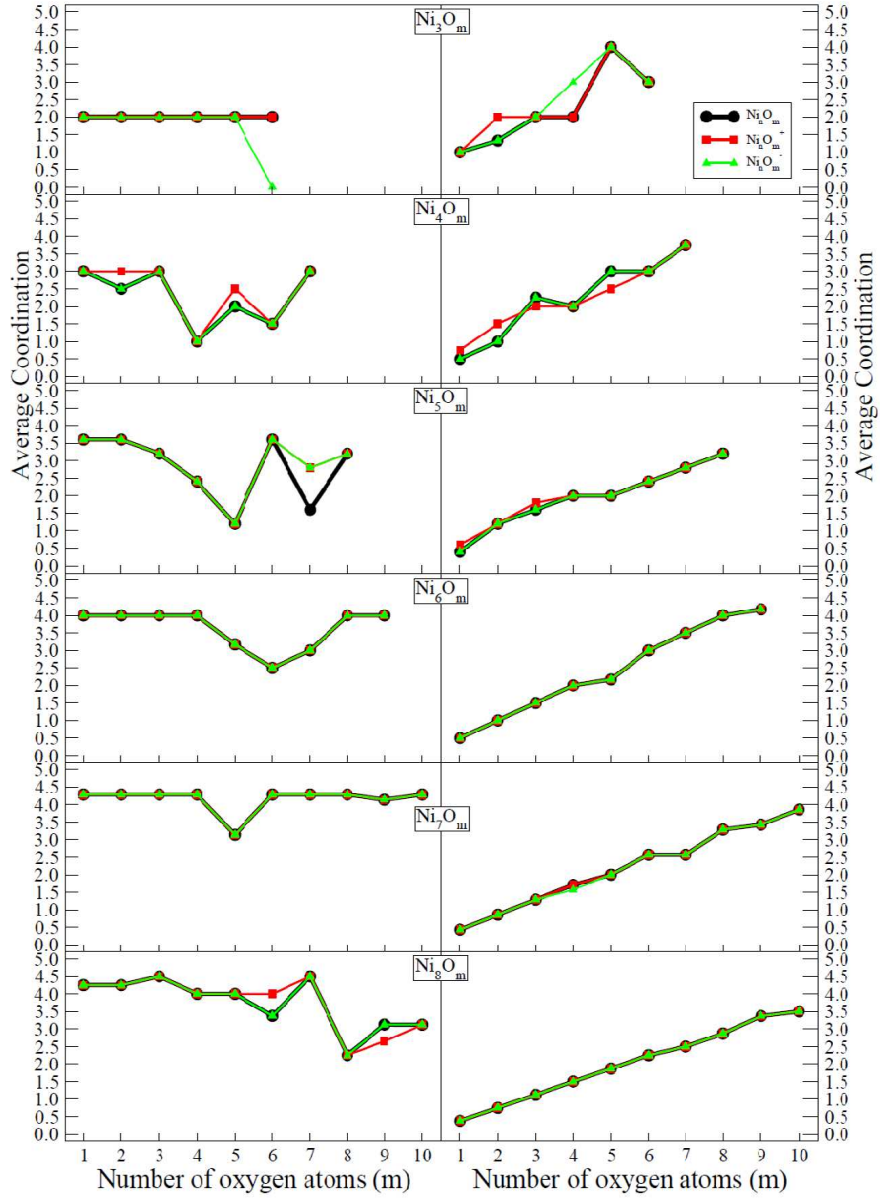


FIG. 8: (Color online) Average Ni-Ni (left) and Ni-O (right panels) coordination of the Ni_nO_m^+ clusters as a function of the number of oxygen atoms (m).

precursor and its possible fragments, and then we consider only the smaller values of these energy differences (excitation energies) within a narrow window of energy. In some cases, due to the aforementioned structural reorganization before fragmentation, we will consider also the energies of the low lying energy isomers given in Tables V-V. Then, our results in this sections give us only a qualitative link between our calculated structures and the

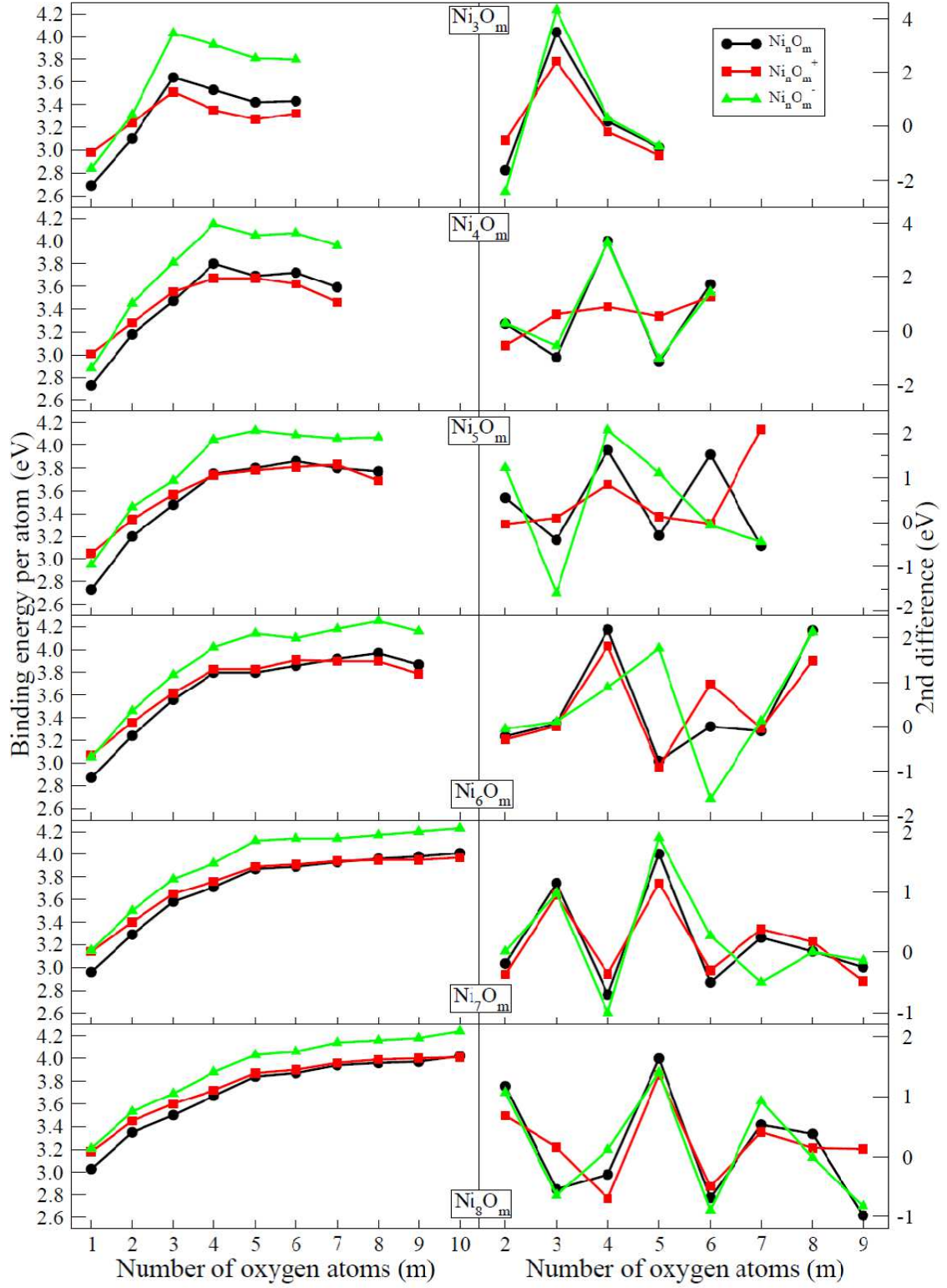


FIG. 9: (Color online) Binding energy per atom (left panels) and second difference of energy (right panels) of $\text{Ni}_n\text{O}_m^{0/\pm}$ clusters as a function of the number of oxygen atoms (m).

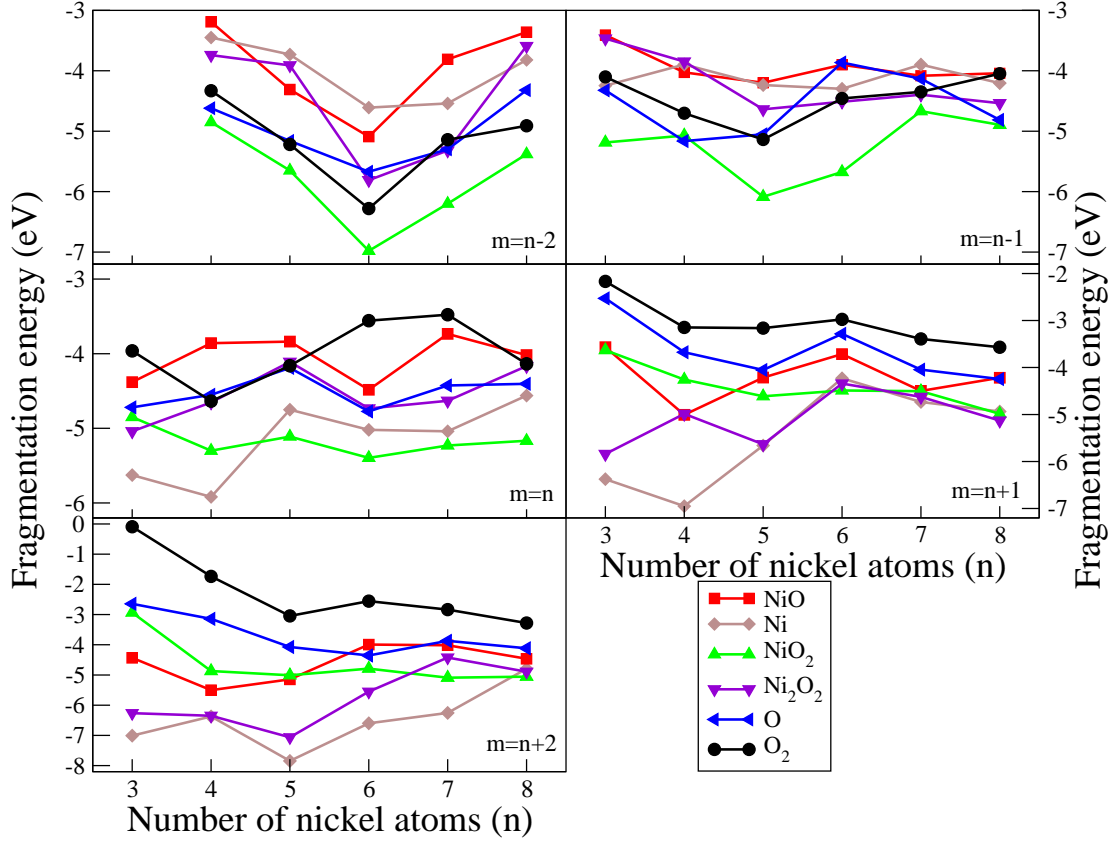


FIG. 10: (Color online) Calculated minimum energy needed to split a Ni_nO_m^+ cation ($m = n \pm 2, n \pm 1, n$) in a neutral and a charged fragment, being the neutral fragment as specified by the code in the lower right panel.

observed photo-fragmentation of cationic nickel oxide clusters.

We will consider the fragmentation of a Ni_nO_m^+ cluster in a neutral fragment plus a charged fragment according to the following channels (in parenthesis is given the symbol used in the Figure 10):

- i) $\text{Ni} + \text{Ni}_{n-1}\text{O}_m^+$; (brown diamonds)
- ii) $\text{NiO} + \text{Ni}_{n-1}\text{O}_{m-1}^+$; (red squares)
- iii) $\text{NiO}_2 + \text{Ni}_{n-1}\text{O}_{m-2}^+$; (green up triangles)
- iv) $\text{Ni}_2\text{O}_2 + \text{Ni}_{n-2}\text{O}_{m-2}^+$; (black down triangles)
- v) $\text{O} + \text{Ni}_n\text{O}_{m-1}^+$; (blue left triangles)

and

- vi) $\text{O}_2 + \text{Ni}_n\text{O}_{m-2}^+$ (black filled circles).

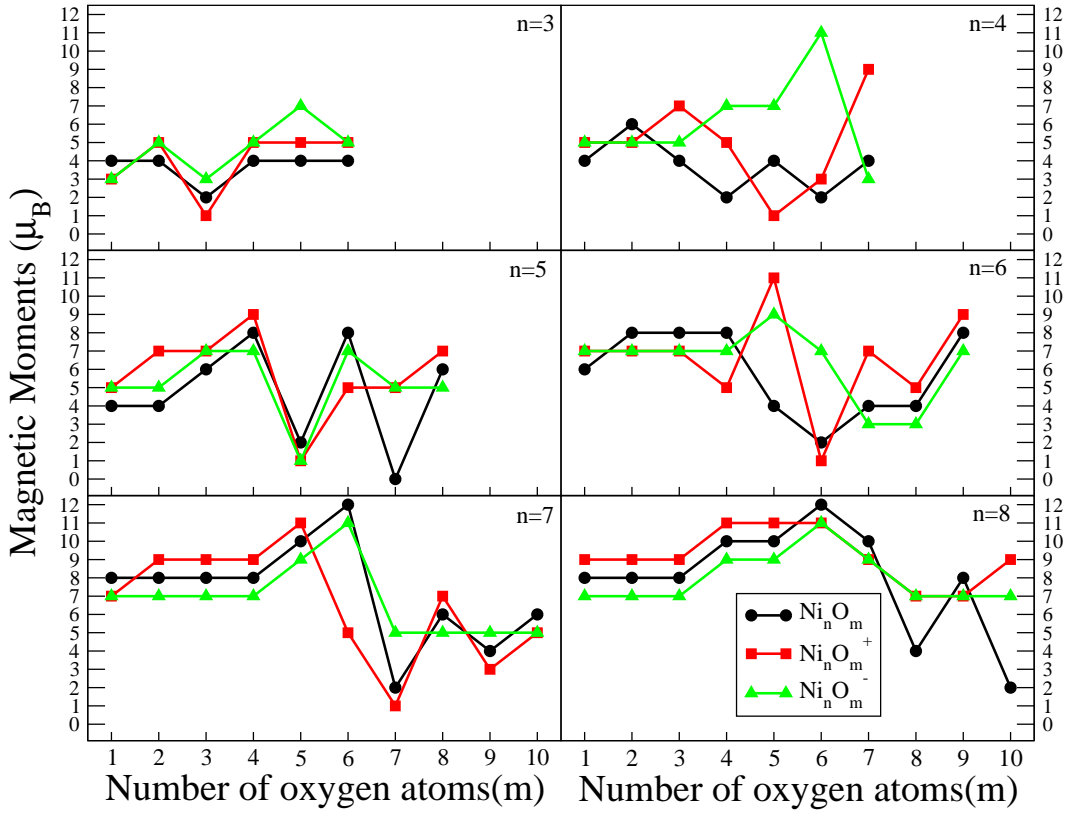


FIG. 11: (Color online) Total spin magnetic moment of $\text{Ni}_n\text{O}_m^{0/\pm}$ clusters as a function of the number of oxygen atoms (m)

In Figure 10 is plotted, as a function of the number of Nickel atoms, the calculated minimum energy needed to produce the fragmentation of Ni_nO_m^+ cations with $n = 3-8$ and $m = n-2$ (panel a), $m = n-1$ (panel b), $m = n$ (panel c), $m = n+1$ (panel d), and $m = n+2$ (panel e). These energies are defined as $E(\text{Ni}_n\text{O}_m^+) - E(\text{Ni}) - E(\text{Ni}_{n-1}\text{O}_m^+)$, for channel i), and similarly for the other ii)-vi) fragmentation channels. In this work are not calculated possible fission barriers which may increase the energy needed for some fragmentation channels.

First we check our results against two general features which were highlighted in the experimental results of Duncan and coworkers¹⁸:

I) Mostly of the experimental photo-fragmentation series for $n.m+2$, $n.m+1$, and $n.n$ (the $n.n-1$ series were not observed) contain the $n.m-2$ fragment, which corresponds to the release of O_2 . The few exceptions are the 3.6, 6.6, and 8.8 fragmentation series. That experimental feature is reproduced by our calculations, that is, the loss of O_2 , is always the channel



estequiometrias

FIG. 12: (Color online) Energy difference (with respect to our putative ground state) as a function of the spin state of several structural arrangements of the stoichiometric clusters $\text{Ni}_n\text{O}_n^{0/+}$.

requiring minimum energy for the fragmentation series $n.m+2$, $n.m+1$, and $n.n$, as seen in Figure 10. The only exceptions are the fragmentation of 5.5, 4.4, and 8.8 parent cations, the last one in agreement with experiments. For these cases, the fragments 4.4, 3.3, and 7.7, respectively, are preferred to 5.3, 4.2, and 8.6 ones, respectively, as can be seen in the panel $m=n$ of Figure 10). Notice that the predicted as preferred fragments, namely 4.4, 3.3, and 7.7, are also observed in the experimental fragmentation of 5.5, 4.4, and 8.8 cations.

II) The fragment 2.1 appears in all the experimental dissociation series, except for the



Ni4O4.pdf

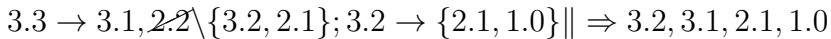
FIG. 13: (Color online) Atomic structures, total spin magnetic moment, local magnetic moments distributions and magnetic couplings of the different spin isomers of $\text{Ni}_4\text{O}_4^{0/\pm}$. Distances in \AA and magnetic moments in μ_B .

8.8 one²⁸. In our calculations, the fragment 2.1 is always obtained too, as we will see later when studying the sequential fragmentation of the several n.m cations. On the other hand, the fragment 1.0 appears together with the fragment 2.1 in all the experimental n.m series with $n < 7$ (except for 6.7 and 5.7), whereas the fragment 1.1 never is detected. In this respect, from our calculations we obtain that the minimum energy for the dissociation $\text{NiO}_2 \rightarrow \text{Ni}^+ + \text{NiO}$ is 3.64 eV, to be compared with at least 5.06 eV needed for the reaction

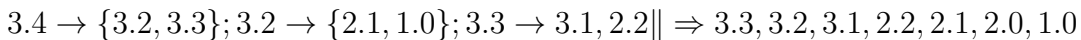
$Ni_2O \rightarrow Ni_2^+ + O$, or with 5.09 eV for $NiO_2 \rightarrow NiO^+ + Ni$ one.

In the following, for each initial parent cation, n.m, we trace the sequential series of fragmentation products by following the lower excitation energy paths along the corresponding panels of Figure 10. Then, we compare these fragments with those from experiments listed in Table 2 of Duncan and coworkers¹⁸. If a predicted fragment is not in that list it is denoted by the symbol $\underline{x,y}$, and then we look into the next most probable fragmentation channel. Reasons for the missing of such fragments are given after each fragmentation chain, usually the plausible existence of a high energy barrier due to large configurational changes. If more than one reaction channel is possible within a narrow window of excitation energy, all the possible fragments are grouped in curly brackets. Then we follow the corresponding sequential series for each of them. If along these sequences appears an already studied (smaller) fragment, we remite us to the already studied series (if both have comparable available energy). In same cases we consider not only the more favorable channel because there are another channels close in energy. Then, the corresponding fragment (or fragments) are separated by a "\ " symbol. All the stable fragments resulting from the application of the rules above are collected after the symbol "\|" and compared with the experimental photo-fragments listed by Duncan and coworkers¹⁸. If an observed fragment is not found following the outlined procedure then it is marked as n.m.

Let us start the procedure above by studying the fragmentation of the 3.3 cation.

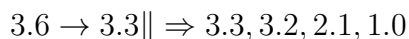


The fragmentation of 3.3 towards 3.2 requires 0.8 eV (0.5 eV) more energy than that to yield the observed 3.1 (unobserved 2.2) fragment. We guest that the dissociation from 3.3 towards 2.2 fragment after excitation with ~ 4.5 eV, may be impeded by a high energy barrier, due to large structural changes (**compare the average bond distances**). On the other hand, 2.1 appears as a fragment of 3.3 as well as a fragment of the intermediate 3.2. This is consistent with the enhancement of the 2.1 signal observed in the experiments.

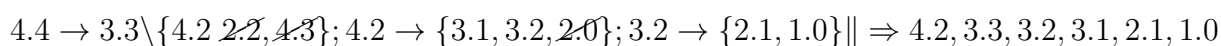


The fragment 2.2, which is not observed in the photo-fragmentation of the 3.3 cation

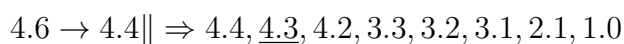
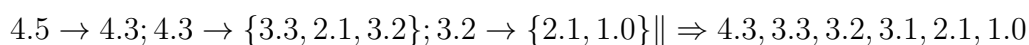
at more than 4.5 eV, may be produced now from dissociation of an excited 3.3* isomer without energy barrier. For example, the isomer 3.3.III, with 1.38 eV higher energy than the 3.3.I G.S. (see Table V, may be reachable at the minimum excitation energy of 3.4 to produce 3.2 (about 2.3 eV), and then dissociate to 2.2 cation by further excitation up to 3 eV. In other words, we are assuming that the cross section of 3.3 to yield the 2.2 fragment is larger in the energy region below 4.0 eV than in the energy region above 4 eV.



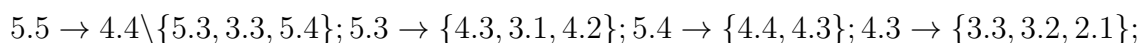
In this especial case with $m=n+3$, the fragment 3.4 is not observed. We guess that the dissociation of 3.6 into 3.4 plus O_2 is hindered by a high energy barrier due to strong geometric changes. The calculated excitation energy to obtain the fragment 3.4 from 3.6 is 1.28 eV, whereas the fragmentation of 3.6 into O_3 and the cation 3.3.III (3.3*) requires only 1.24 eV. Thus, 3.6 may lose its preformed ozonic O_3 unit (see Figure 1) leaving a 3.3* fragment which further decays to 3.3 and becomes fragmented as shown above.



The fragments 2.2 and 4.3 are not observed in this series although the required excitation energy is similar to that producing 4.2. This may be due to high dissociation barriers needed to change from planar to three dimensional geometries (see also the average bond distances of parent and products in Figure 9).



The observed fragments 4.3 may be produced by 4.5 which is not observed, however, in this series. We guess that 4.5 may be produced in an isomeric state which totally dissociates to yield the 4.3 and 4.4 fragments.



4.2 \rightarrow {3.1, 3.2, 2.0}; 3.2 \rightarrow {2.1, 1.0} || \Rightarrow 5.4, 5.3, 4.4, 4.3, 4.2, 3.3, 3.2, 3.1, 2, 2, 2.1, 2.0, 1.0

5.6 \rightarrow {5.4, \{5.5, ~~4.5~~\}}; 5.4 \rightarrow {4.3, 4.4}; 4.3 \rightarrow {3.2, 3.3, 2.1}
 || \Rightarrow 5.5, 5.4, 4.4, 4.3, 4.2, 3.2, 3.1, 2.1, 1.0

The average Ni-Ni (Ni-O) distance is much larger (near equal) in 4.5 than in 5.6, so a high barrier may occur for that fragmentation.

5.7 \rightarrow 5.5 || \Rightarrow 5.5, 5.4, 5.3, 4.4, 4.3, 4.2, 3.3, 3.2, 3.1, ~~2, 2~~, 2.1, ~~2.0, 1.0~~

The experimental fragmentation of 5.7 does not shows the cations 2.2, 2.0, and 1.0. A possible reason is that these small fragments, when coming from the 5.5 series, are produced only if a minimum energy (4.3 eV) is available to yield 4.3 and 3.3 fragments. However, 5.5 may be produced from 5.7 cation by a minimum excitation energy of \sim 2.7 eV, which is not sufficient to fragment further the 5.5 cation into 4.3 and 3.3.

6.6 \rightarrow ~~6.4~~ \{5.5\} {6.5, 5.4}; 6.5 \rightarrow {5.4, ~~6.4~~}; 5.4 \rightarrow {4.3, 4.4}; 4.3 \rightarrow {2.1, 3.3, 4.2}; 4.2 \rightarrow {3.1, 3.2, 2.0}; 3.2 \rightarrow {2.1, 1.0} || \Rightarrow 6.5, 5.4, 5.3, 4.4, 4.3, 4.2, 3.3, 3.2, 3.1, 2.2, 2.1, 2.0, 1.0

The minimum energy to obtain the 6.4 fragment is about 3.6 eV, and for the 5.5 and 6.5 fragments it is about 4.4 eV. The 6.4 and 5.5 are not observed because high energy barriers may occurs due to geometrical factors, considering the average bond distances of 6.m clusters, on one hand, and the planar geometry of 5.5 on the other hand. Instead the observed 5.3 cation may be produced by exciting 5.4 to energy higher than 5 eV.

6.7 \rightarrow {6.5, ~~6.6~~}; 6.5 \rightarrow {~~6.4~~, 5.4}; 5.4 \rightarrow {4.3, ~~4.4~~}; 4.3 \rightarrow {2.1, 3.3, 3.2}; 3.2 \rightarrow {2.1, ~~1.0~~}
 || \Rightarrow 6.5, 5.4, 4.3, 4.2, 3.3, 3.2, 3.1, 2.1, 2.0

The observed 2.0 fragment can be produced from 2.1 providing a minimum excitation energy of 5.06 eV.

7.7 \rightarrow {7.5, ~~6.6~~}; 7.5 \rightarrow 6.4; 6.4 \rightarrow {5.4, 5.3}; 5.4 \rightarrow {4.3, 4.4}; 4.3 \rightarrow {2.1, 3.3, 3.2};
 3.2 \rightarrow {2.1, 1.0} || \Rightarrow 7.5, 6.4, 5.4, 5.3, 4.4, 4.3, 4.2, 3.3, 3.2, 3.1, 2.1, 2.0

The fragment 4.2 may be produced from the intermediate 5.4 excited to more than 6 eV but then it should appear also the unobserved 5.2 fragment.

$$\begin{aligned}
7.8 &\rightarrow 7.6; 7.6 \rightarrow \{\cancel{6.6}, 6.5, 7.5\} \setminus \{\cancel{7.4}, 5.4, 6.4\}; 7.5 \rightarrow 6.4; 6.5 \rightarrow \{6.4, 5.4\}; \\
6.4 &\rightarrow \{5.4, 5.3\}; 5.4 \rightarrow \{4.3, 4.4\}; 4.3 \rightarrow \{2.1, 3.3, 3.2\}; 3.2 \rightarrow \{2.1, 1.0\} \\
\parallel &\Rightarrow 7.6, 7.5, 6.5, 6.4, 5.4, 5.3, 4.4, 4.3, \underline{4.2}, 3.3, 3.2, 3.1, 2.1, 2.0
\end{aligned}$$

$$8.8 \rightarrow \{7.7, \cancel{8.6}\} \parallel \Rightarrow 7.7, 7.5, \cancel{6.6}, \underline{6.5}, \cancel{6.4}, 5.4, \cancel{5.3}, \cancel{4.4}, 4.3, \underline{4.2}, 3.3, 3.2, 3.1, 2.1, 2.0$$

The fragments 4.2 and smaller than 4.2 are not reported in the experiments^{18,28}.

$$\begin{aligned}
8.9 &\rightarrow 8.7 \rightarrow 7.6 \rightarrow \{\cancel{6.6}, 6.5, \cancel{7.5}\}; 6.5 \rightarrow \{5.4, \cancel{6.4}\}; 5.4 \rightarrow \{4.3, 4.4\}; 4.3 \rightarrow \{2.1, \cancel{3.3}, 4.2\}; \\
4.2 &\rightarrow \{\cancel{3.1}, 3.2, \cancel{2.0}\}; 3.2 \rightarrow 2.1, \cancel{1.0} \parallel \Rightarrow 8.7, 7.6, 6.5, 5.4, 4.4, 4.3, 2.1, 4.2, 3.2, 2.1
\end{aligned}$$

In this section we have qualitatively explained how mostly of the observed n.m photo-fragments appears due to simple final state energetic considerations. The exceptions are possibly due to the existence of high energy barriers which impede large configurational changes.

C. Magnetic properties

In Fig.11 we summarize the results obtained for the total spin magnetic moment of the investigated Ni_nO_m clusters in their neutral and charged states. For most clusters, the change in the spin state upon ionization or upon an electron excess is consistent with a one electron process (reduction or increase of $1\mu_B$ with respect to charge neutrality). However, we note that Ni_4O_m is an exception in which for most oxidation rates, one electron more or less implies a strong spin-dependent charge redistribution leading to a large change of spin state. In this case, Ni_4O_6 is particularly relevant, since an electron excess increases the total spin moment from $2\mu_B$ (in the neutral state) to $11\mu_B$, that is a high spin state. It is interesting to note that the total moment of pure Ni_4 is $4\mu_B$ in our approach (in agreement with gaussian results²⁷), so that the oxidation at this rate ($m = 6$) did not significantly change the magnetic moment of Ni_4 , but an electron excess in addition did it. This huge

increase is not accompanied, in this case, by a noticeable change of the structural shape as in other clusters (see Tables I-XII of the SI). Therefore, in order to analyze the origin of such dramatic change in the total moment, we have calculated the atom-projected spin-polarized charge density and assigned local magnetic moments to the different atoms of the cluster, according to mulliken populations (the same for the electronic occupation). The low spin state of the neutral Ni_4O_6 is due to antiparallel couplings which transform, upon the electron excess, into a ferromagnetic-like arrangement with Ni moments of $1.46\mu_B$ (more than twice the local moment of a Ni atom in the fcc bulk) and O moments of $0.86\mu_B$, and the resulting huge total moment. This cluster Ni_4O_6^- , as well as others like Ni_6O_5^+ , Ni_7O_6 and Ni_8O_6 , are specially interesting in the context of magnetic grains because of their large total magnetic moment (11 or $12\mu_B$). In particular, the last three ones are among the most abundant ones according to their stoichiometry in connection with mass spectrometry and photodissociation experiments¹⁸. Moreover our results demonstrate that the unavoidable oxidation in environmental conditions does not necessarily quench the magnetic moment. On the contrary, the huge total moment of Ni_7O_6 and Ni_8O_6 is due to oxidation, since the neutral Ni_7 and Ni_8 clusters have lower magnetic moment. And in the case of Ni_8O_6 the moment is even robust against both ionization and electron excess.

Fig.11 demonstrates that oxidation does not quench, in general, the magnetic moment of small Ni clusters. From the local moments distribution within the clusters, we identified a high spin-polarization in many Ni atoms and a noticeable spin-polarization of O in general, which contributes the total magnetic moment. Other Ni atoms have low moments, close to the value in fcc bulk or even lower. We also find that changes in the spin state due to the charge state are not necessarily accompanied by a change of structural shape (an example being the cluster Ni_4O_6 , already discussed) and no systematic trends are obtained from the data in this regard (see Tables I-XII of the SI). In general, most Ni oxide clusters exhibit antiparallel magnetic couplings in a more or less degree. Antiparallel couplings are a clear signature of strong Ni-O interaction and oxygen-mediated Ni-Ni exchange, since pure Ni clusters are ferromagnetic-like. Clusters with larger total moment are those with less antiparallel couplings, thus closer to the ferromagnetic-like arrangement with high local spin-polarization. However, there exist few Ni oxide clusters with a small total moment (examples are Ni_6O_5 , and Ni_nO_n with $n = 3$ and 6 discussed later) but which exhibit a ferromagnetic-like configuration instead of antiparallel couplings, although with low local spin-polarization

(Ni moments smaller than in the bulk). Analyzing the trend of the total spin moment as a function of the oxidation rate, we clearly see that it is non-monotonous, and that, in general, a minimum in the total moment is reached at the stoichiometric oxidation rate ($n = m$). This means that from the magnetic point of view, if a large magnetic moment is desired, oxidation at the stoichiometric rate must be avoided, but this seems difficult. In fact, mass spectrometry and photodissociation experiments¹⁸ revealed that stoichiometric clusters are among the most abundant ones. Ion mobility mass spectrometry¹⁹ revealed a transition from two-dimensional ring- to tri-dimensional compact- structures in Ni_nO_n^+ and $\text{Ni}_n\text{O}_{n-1}^+$ at $n = 5$. They also found that both types of structures coexist for Ni_5O_5^+ . Calculations of the same group¹⁹ were consistent with the above facts in terms of cross sections which fitted the experimental values. However, for Ni_4O_4^+ the ring structure, although having the correct cross-section, is not their putative ground state; For Ni_5O_5^+ the ring structure is even at 0.36eV above the ground state which is relatively compact, but not the cluster with the correct cross section (the compact isomer with cross section closer to the experimental value is also quite high in energy, at 0.34eV above the ground state). Isomers at such high energy with respect to the ground state are not expected to be present for this size.

Since stoichiometric clusters are relevant due to their abundance (relative stability) and in view of the facts discussed above, it is pertinent to revisit them in some detail. We have analyzed the stoichiometric clusters found in our approach, in both the neutral (Ni_nO_n) and the cationic (Ni_nO_n^+) states (the experiment deal with cations). In Fig.12 we report the energy difference (with respect to our putative ground state) as a function of the spin state for all those clusters, considering several structure types. The main trends are: (i) two-dimensional ring structures are the putative ground state up to $n = 5$ for both charge states, which provides consistency with experiments of Ion mobility mass spectrometry¹⁹ also from the energetic point of view. The compact structures calculated by Ohshimo *et al.*¹⁹ as the putative ground state of Ni_4O_4^+ and Ni_5O_5^+ are now our first isomers; (ii) a transition to compact three-dimensional structures, based on an octahedron Ni subcluster, takes place at $n = 6$. Those compact structures are more competitive with the ring ones in the cationic clusters than in their neutral counterparts, as demonstrated by the fact that spin- and structural-isomers start to be accessible at the same energy window for smaller sizes in cationic clusters than in neutral ones; (iii) A further structural transition takes place at $n = 8$, where the pattern based on an octahedron Ni subcluster evolves to a more open

structure, again for the two charge states; (iv) a magnetic transition is found to occur just at $n = 8$ corresponding to the mentioned loss of the structural pattern based on the octahedron Ni subcluster. Thus, neutral clusters change from a total spin magnetic moment of $2\mu_B$ to $4\mu_B$, while cationic clusters change from $1\mu_B$ (being Ni_4O_4^+ the only exception with $5\mu_B$) to $7\mu_B$. Due to the relevance of Ni_4O_4 and to its being an exception in the magnetic trend, we discuss it in more detail at the end of this section.

Our results indicate that, for small Ni clusters oxidized at the stoichiometric rate, the geometrical shape does not essentially change upon ionization (just structural relaxations take place, as we will see in detail for Ni_4O_4 at the end of this section). From the data reported in Tables I-XII of the supplementary information, we see that an electron excess does not affect essentially the structure either. We note that the above can not be generalized to oxidation rates other than the stoichiometric one; on the contrary, the equi-atomic concentration seems to be an exception, since the ground state structures strongly depend on the charge state in a considerable number of non-stoichiometric Ni oxide clusters, particularly for those with $n < 7$ (see Tables I-XII of the SI). In fact, stoichiometric clusters are an exception also in regard to the magnetic properties. These clusters, in their neutral and cationic states, bear the lowest total spin magnetic moment among the investigated compositions. They are in a low spin state before the second structural transition takes place. Note, however, that stoichiometric Ni oxides in the anionic state bear a higher spin magnetic moment. The change in the spin state upon ionization in stoichiometric Ni oxide clusters is consistent with a one electron process (reduction of $1\mu_B$), except for $n = 8$, being this cluster particularly interesting since ionization produces just the opposite effect, that is a spin-polarized electronic redistribution leading to a relatively high magnetic moment of $7\mu_B$. The same trend is obtained for the anionic state, indicating that an electron excess does produce a strong spin-dependent electronic charge redistribution, regardless the slight relaxation of the atomic structure.

Different spin-dependent electronic charge distribution can lead to the same total spin moment of the system. It is pertinent to explore the origin of the resulting total moment, in terms of magnetic couplings and local spin-polarizations. The origin of the low spin state in stoichiometric Ni_nO_n is not the same for all n . For $n = 3$ and 6, the clusters exhibit a ferromagnetic-like arrangement with all local moments pointing in the same orientation, but with a small spin-polarization in the Ni sites (0.32 and $0.22\mu_B$ for $n = 3$ and 6, respectively,

about half the value in the fcc bulk) and an important contribution from the O sites (0.35 and $0.12\mu_B$ for $n = 3$ and 6 , respectively). Interestingly, Ni_6O_6 is formed by two Ni_3O_3 rings. These are exceptional cases, since most of the clusters exhibit antiparallel magnetic couplings, in more or less degree, with some Ni local moments that can reach up to about $1.3\mu_B$, that is about twice the local moment of a Ni atom in the fcc bulk.

Finally, we analyze in detail the spin isomers of Ni_4O_4 . For the sake of brevity, we don't present a similar analysis for other clusters (the reader can obtain the data from the authors upon request). Fig.13 illustrates the atomic structures, local magnetic moments distributions and magnetic couplings of the different spin isomers of Ni_4O_4 , Ni_4O_4^+ and Ni_4O_4^- . As discussed above, the atomic structure is a two-dimensional ring, independently of the spin and charge states. Local relaxations are concomitant with the symmetry imposed by the spin-polarized charge distribution. Thus, ferromagnetic-like clusters (those with the higher total spin moment) are highly symmetric (see the high-spin states in all charge states). Symmetry breaking takes place as soon as antiparallel couplings arise. Marked antiferromagnetic-like configurations lead to low-spin states. These trends are common to all Ni oxide clusters investigated here, as discussed in previous paragraphs. We also find that different spin isomers with the same magnetic couplings exist, in which case the difference comes from the local spin-polarization (compare, for instance the local moments in the neutral Ni_4O_4 with total moments of 4, 6 and 8, all corresponding to ferromagnetic-like configurations). We can also identify spin-isomers whose energy difference essentially comes from the electronic redistribution, with atomic structure practically unchanged, while in other cases, part of this energy difference is contributed by the noticeable structural relaxation (the two lower-spin states of Ni_4O_4 and Ni_4O_4^+).

IV. CONCLUSIONS

Acknowledgments

We acknowledge the support of the Spanish Ministry of Economy and Competitiveness and the European Regional Development Fund (Project FIS2014-59279-P). F.A-G acknowledges financial support from PROMEP-SEP-CA230. R.H.A-T acknowledges the financial support provided by the University of Valladolid for a research visit and a fellowship from

CONACyT (Mexico, scholarship 415121).

* avega@fta.uva.es

- ¹ F. Piccinno, F. Gottschalk, S. Seeger, B. Nowack, J. Nanopart. Res **14**, 1109 (2012)
- ² A.A. Keller, S. Mc.Ferran, A. Lazareva, S. Suh, J. Nanopart. Res **15**, 1692 (2013)
- ³ K.P. Kühn, I.F. Cahbemy, K. Massholder *et al.*, Chemosphere **53**, 71 (2003)
- ⁴ G. Rajakumar, A.A. Rahuman, S.M. Roopan *et al.*, Spectrochim Acta A **91**, 23 (2012)
- ⁵ M.A. Vargas-Reus, K. Memarzadeh, J. Huang, G.G. Ren, R.P. Allaker, Int. J. Antimicrob. Agents **40**, 135 (2012)
- ⁶ S. Martel, J. Nanopart. Res. **17**, 55 (2015).
- ⁷ R.H. Kodama, J. Mag. Mag. Mat. **200**, 359 (1999).
- ⁸ A.H. Lu, E.L. Salabas, F. Schueth, Angew. Chem. Int. Ed. **46**, 1222 (2007).
- ⁹ C.J. Jia, M. Schwickardi, C. Weidenthaler, W. Schmidt, S. Korhonen, B.M. Weichuysen, F. Schueth, J. Am. Chem. Soc. **133**, 11279 (2011).
- ¹⁰ N.F. Atta, A.H. Ibrahim, and A. Galal, New J. Chem. **40**, 662 (2016).
- ¹¹ P. Poizot, S. Laruelle, S. Grugeon, L. Dupont, J.M. Tarascon, Nature **407**, 496 (2000).
- ¹² G. Eranna, B.C. Joshi, D.P. Runthala, R.P. Gupta, CRC Crit. Rev. Solid State **29**, 111 (2004).
- ¹³ I. Kobal, M. Senegacnik, H. Kobal, J. Catal. **49**, 1 (1977).
- ¹⁴ G.A. El-Shobaky, A.M. Ghozza, Mater. Lett. **58**, 699 (2004).
- ¹⁵ W. Yao, C. Huang, J. Ye, Chem. Mater. **22**, 1107 (2010).
- ¹⁶ X. Shu, J. He, D. Chen, Ind. Eng. Chem. Res. **47**, 4750 (2008).
- ¹⁷ C.U. Mordi, M.A. Eleruja, B.A. Taleatu, G.O. Egharevba, A.V. Adedeji, O.O. Akinwunmi, B. Olofinjana, C. Jeynes, and E.O.B. Ajayi, J. Mater. Sci. Tech., **25**, 85 (2009).
- ¹⁸ C.J. Dible, S.T. Akin, S. Ard, C.P. Fowler, and M.A. Duncan, J. Phys. Chem. A **116**, 2691 (2012).
- ¹⁹ K. Ohshimo, A. Azuma, T. Komukai, R. Moriyama, and F. Misaizu, J. Phys. Chem. C **119**, 11014 (2015).
- ²⁰ J. M. Soler, E. Artacho, J. D. Gale, A. García, J. Junquera, P. Ordejón, and D. Sánchez-Portal, J. Phys.: Condens. Matter **14**, 2475 (2002).
- ²¹ J. P. Perdew, K. Burke, and M. Ernzerhof, Phys. Rev. Lett. **77**, 3865 (1996).

TABLE I: Several properties of neutral nickel oxide clusters: Sym = molecular symmetry; $E_b(n, m)$ = binding energy per atom in eV; μ = magnetic moment in Bohr magnetons (μ_B); I_p = ionization potential in eV; H-L = Kohn-Sham Homo-Lumo gap in eV.

Signature <i>n.m</i> -isomer	<u>neutral</u>						
	Sym	$E_b(n, m)$	I_p	E_a	μ	D(Ni-Ni)	D(Ni-O)
3.1-I	C_{3v}	2.69	6.56	0.72	4	2.38	1.94
3.1-II	C_s	2.66	7.01	1.10	4	2.34	1.84
3.1-III	C_{2v}	2.49	7.46	1.59	4	2.29	1.70
3.2-I	C_{2v}	3.01	6.99	1.20	2	2.50	1.97
3.2-II	C_s	3.11	7.15	1.47	4	2.43	1.92
3.2-III	C_s	3.16	7.54	2.13	4	2.46	1.82
3.3-I	D_{3h}	3.64	8.50	2.47	2	2.44	1.80
3.3-II	$C_{\infty v}$	3.27	7.57	2.59	2	-	1.74
3.3-III	C_s	3.33	7.98	2.56	4	2.55	1.85
3.4-I	C_s	3.52	8.66	2.95	4	2.52	1.81
3.4-II	C_{3v}	3.56	8.90	2.94	2	2.54	1.89
3.4-III	C_1	3.30	8.32	4.47	2	2.60	1.89
3.5-I	D_{3h}	3.42	8.98	3.23	4	2.53	1.94
3.5-II	C_1	3.36	9.45	4.17	6	2.67	1.88
3.6-I	C_s	3.43	8.74	3.49	4	2.83	1.87
3.6-II	C_s	3.44	9.69	4.49	4	3.23	1.76

²² N. Troullier, and J.L. Martins, Phys. Rev. B **43**, 1993 (1991).

²³ L. Kleinman and D. M. Bylander, Phys. Rev. Lett. **48**, 1425 (1982).

²⁴ S. G. Louie, S. Froyen, and M. L. Cohen, Phys. Rev. B **26**, 1738 (1982).

²⁵ G. Kresse and J. Furthmüller, Phys. Rev. B. **54**, 11169 (1996).

²⁶ G. Kresse and J. Hafner, Rev. B. **47**, R558 (1993).

²⁷ S. Goel, A.E. Masunov, J. Mol. Model. **18**, 783 (2012).

²⁸ M.A. Duncan, private communication: the entry 3.3 in Table 2 of Duncan and coworkers¹⁸ contains the 3.3 fragment instead of the 3.1 one, due to a misprint. Also, in the entry 8.8 any fragments smaller than 4.3 were not detected, and those larger than 4.3 shows a very weak signal

V. APPENDIX

TABLE II: Several properties of cationic and anionic nickel oxide clusters: Sym = molecular symmetry; $E_b(n, m)$ = binding energy per atom in eV; μ = magnetic moment in Bohr magnetons (μ_B); I_p = ionization potential in eV; H-L = Kohn-Sham Homo-Lumo gap in eV.

Signature				cation/anion	
$n.m$ -isomer	Sym	$E_b(n, m)$	μ	D(Ni-Ni)	D(Ni-O)
3.1-I	C_{3v}/C_1	2.98/2.84	3	2.44/2.42	1.89/1.92
3.1-II	C_{3v}/C_s	2.83/2.90	3	2.57/2.32	1.78/1.88
3.1-III	C_s/C_{2v}	2.55/2.85	5/3	2.34/2.28	1.74/1.72
3.2-I	D_{3h}/C_{2v}	3.24/3.31	5	2.58/2.57	1.96/1.99
3.2-II	C_s	3.22/3.38	5	2.62/2.42	1.91/1.95
3.2-III	C_{2v}/C_s	3.20/3.56	5	2.89/2.46	1.81/1.85
3.3-I	D_{3h}	3.51/4.03	1/3	3.12/2.51	1.79/1.82
3.3-II	$C_{\infty v}$	3.29/3.68	3/5	- / -	1.75/1.76
3.3-III	C_s	3.28/3.73	1/5	2.73/2.17	1.85/1.89
3.4-I	C_s	3.38/3.92	5	2.70/2.51	1.81/1.83
3.4-II	C_s/C_{3v}	3.35/3.95	5	2.79/2.51	1.89/1.94
3.4-III	$C_1/ -$	3.22/ -	5/-	2.74/ -	1.90/ -
3.5-I	D_{3h}	3.27/3.81	5/3	2.60/2.48	1.92/1.96
3.5-II	C_1/C_s	3.14/3.86	7	2.72/2.62	1.88/1.90
3.6-I	C_s	3.32/3.80	5/3	2.92/2.74	1.87/1.87
3.6-II	C_s/C_1	3.22/3.93	7/5	3.35/3.29	1.77/1.77

TABLE III: Several properties of neutral nickel oxide clusters: Sym = molecular symmetry; $E_b(n, m)$ = binding energy per atom in eV; μ = magnetic moment in Bohr magnetons (μ_B); I_p = ionization potential in eV; H-L = Kohn-Sham Homo-Lumo gap in eV.

Signature <i>n.m</i> -isomer	<u>neutral</u>						
	Sym	$E_b(n, m)$	I_p	E_a	μ	D(Ni-Ni)	D(Ni-O)
4.1-I	C_{3v}	2.73	6.30	0.90	4	2.38	1.97
4.1-II	C_{2v}	2.76	6.55	1.06	4	2.41	1.83
4.1-III	C_{2v}	2.62	6.89	1.72	6	2.34	1.82
4.2-I	C_s	3.18	7.12	1.72	6	2.50	1.90
4.2-II	C_s	3.17	7.36	2.44	4	2.49	1.81
4.2-III	C_{2v}	3.19	7.55	2.33	6	2.48	1.82
4.3-I	C_s	3.47	7.13	2.52	0	2.50	1.83
4.3-II	C_{3v}	3.42	6.81	1.85	2	2.60	1.94
4.3-III	C_s	3.52	7.52	2.41	4	2.48	1.85
4.4-I	C_{2v}	3.80	8.09	3.53	2	2.68	1.79
4.4-II	T_d	3.74	7.73	1.61	0	2.71	1.98
4.4-III	C_{3v}	3.75	8.00	2.54	8	2.71	1.87
4.5-I	C_{2v}	3.69	7.89	3.30	2	2.76	1.81
4.5-II	C_{2v}	3.75	8.44	3.09	4	2.81	1.89
4.5-III	C_{2v}	3.66	7.64	3.56	4	2.55	1.82
4.6-I	C_2	3.72	8.72	3.61	2	2.92	1.83
4.6-II	D_{4h}	3.62	8.11	3.77	6	2.48	1.96
4.6-III	C_s	3.66	8.89	3.62	6	2.66	1.91
4.7-I	C_{3v}	3.59	9.09	4.17	4	2.63	1.89
4.7-II	C_{2v}	3.57	9.49	4.16	6	2.61	1.92

TABLE IV: Several properties of cationic and anionic nickel oxide clusters: Sym = molecular symmetry; $E_b(n, m)$ = binding energy per atom in eV; μ = magnetic moment in Bohr magnetons (μ_B); I_p = ionization potential in eV; H-L = Kohn-Sham Homo-Lumo gap in eV.

Signature <i>n.m</i> -isomer	Sym	$E_b(n, m)$	μ	cation/anion	
				D(Ni-Ni)	D(Ni-O)
4.1-I	C_s	3.01/2.88	5/3	2.52/2.39	1.91/1.97
4.1-II	C_{2v}/C_2	2.99/2.95	5	2.47/2.36	1.82/1.85
4.1-III	C_{2v}	2.78/2.94	5	2.36/2.38	1.81/1.82
4.2-I	C_s	3.28/3.45	5	2.58/2.48	1.86/1.90
4.2-II	$C_s/ -$	3.23/ -	7/-	2.64/ -	1.83/ -
4.2-III	C_{2v}/C_s	3.22/3.56	7/5	2.69/2.39	1.82/1.85
4.3-I	C_s/C_{3v}	3.55/3.81	7/5	2.74/2.46	1.90/1.85
4.3-II	C_{3v}	3.55/3.67	7/5	2.77/2.58	1.95/1.98
4.3-III	C_s	3.55/3.85	7/5	2.75/2.46	1.85/1.87
4.4-I	C_1/D_{4h}	3.67/4.15	5/7	3.23/2.46	1.78/1.82
4.4-II	T_d	3.66/3.85	1/7	2.78/2.69	1.96/2.00
4.4-III	C_{3v}/C_s	3.61/3.97	9/7	2.76/2.56	1.86/1.90
4.5-I	C_{2v}	3.67/4.05	1/3	3.08/2.68	1.78/1.84
4.5-II	C_{4v}/C_s	3.67/4.08	3/7	2.84/2.81	1.89/1.87
4.5-III	C_{2v}/C_s	3.67/4.04	5	3.08/2.64	1.79/1.84
4.6-I	C_{3v}/T_d	3.65/4.07	3/11	3.11/2.75	1.84/1.87
4.6-II	C_{2h}/D_{4h}	3.58/3.98	5	2.79/2.45	1.91/1.99
4.6-III	C_s	3.54/4.01	7/5	2.71/2.64	1.90/1.92
4.7-I	C_{3v}	3.46/3.96	9/3	2.81/2.55	1.89/1.89
4.7-II	C_{2v}/C_s	3.41/3.94	7/5	2.70/2.55	1.92/1.92

TABLE V: Several properties of neutral nickel oxide clusters:

Signature <i>n.m</i> -isomer	neutral						
	Sym	$E_b(n, m)$	I_p	E_a	μ	D(Ni-Ni)	D(Ni-O)
5.1-I	C_{2v}	2.72	5.79	1.48	6	2.44	1.86
5.1-II	C_s	2.81	6.53	1.53	4	2.41	1.81
5.1-III	C_{4v}	2.68	6.06	0.95	4	2.42	1.98
5.2-I	C_s	3.20	6.68	1.98	4	2.55	1.93
5.2-II	C_s	3.19	6.77	2.01	6	2.52	1.89
5.2-III	C_{2v}	3.18	6.90	1.85	6	2.50	1.82
5.3-I	C_s	3.48	6.99	1.82	4	2.57	1.92
5.3-II	C_s	3.46	7.10	2.41	6	2.62	1.85
5.3-III	C_s	3.49	6.40	2.46	6	2.50	1.89
5.4-I	C_{2v}	3.75	7.79	2.87	8	2.56	1.87
5.4-II	C_1	3.68	7.35	2.55	8	2.65	1.92
5.4-III	C_s	3.61	7.99	2.83	4	2.59	1.81
5.5-I	C_{2v}	3.80	7.85	3.56	2	3.08	1.75
5.5-II	C_{2v}	3.74	7.52	2.57	2	2.81	1.95
5.5-III	C_1	3.73	7.61	2.54	2	2.80	1.93
5.5-IV	C_{2v}	3.72	7.44	2.89	2	2.61	1.81
5.6-I	C_{2v}	3.86	8.33	3.54	8	2.79	1.79
5.6-II	C_{3v}	3.80	8.03	3.15	8	2.78	1.91
5.6-III	D_{3h}	3.78	7.85	2.67	6	2.66	1.97
5.7-I	C_{2v}	3.80	7.40	3.79	6	2.98	1.80
5.7-II	C_s	3.83	8.55	3.52	0	2.13	1.85
5.7-III	C_s	3.82	8.54	3.55	4	2.83	1.86
5.8-I	C_s	3.77	8.81	4.06	6	2.98	1.81
5.8-II	C_1	3.73	8.63	3.87	8	2.90	1.91
5.8-III	C_2	3.67	8.93	4.02	6	2.72	1.94

TABLE VI: Several properties of cationic and anionic nickel oxide clusters:

Signature	cation/anion				
$n.m$ -isomer	Sym	$E_b(n, m)$	μ	D(Ni-Ni)	D(Ni-O)
5.1-I	C_s/C_{2v}	3.05/2.95	5	2.51/2.44	1.89/1.88
5.1-II	C_s	3.01/3.04	5	2.45/2.41	1.81/1.85
5.1-III	C_{4v}	2.96/2.83	5/3	2.44/2.43	1.99/1.98
5.2-I	$C_s/ -$	3.35/ -	7/-	2.63/ -	1.93/ -
5.2-II	C_s	3.33/3.46	7/5	2.65/2.44	1.87/1.92
5.2-III	C_{2v}	3.30/3.43	5	2.51/2.49	1.80/1.83
5.3-I	C_s	3.57/3.69	7	2.71/2.58	1.92/1.95
5.3-II	C_s	3.53/3.74	5	2.69/2.53	1.83/1.87
5.3-III	C_s	3.53/3.78	7	2.61/2.51	1.87/1.91
5.4-I	C_s/C_{2v}	3.74/4.05	9/7	2.69/2.53	1.86/1.88
5.4-II	C_s	3.72/3.95	9/7	2.81/2.56	1.91/1.95
5.4-III	C_s	3.58/3.91	5/3	2.65/2.30	1.81/1.84
5.5-I	C_s/D_{5h}	3.78/4.14	1	3.17/2.88	1.75/1.77
5.5-II	C_{2v}	3.77/3.99	3/9	2.84/2.71	1.93/1.96
5.5-III	C_1/C_s	3.76/3.99	5/9	2.90/2.71	1.92/1.96
5.5-IV	C_1	3.75/3.99	11/7	2.90/2.63	1.94/1.92
5.6-I	D_{3h}	3.81/4.09	5/7	2.86/2.80	1.86/1.81
5.6-II	C_s	3.78/4.08	7	2.93/2.77	1.90/1.92
5.6-III	D_{3h}	3.77/4.01	7/5	2.73/2.66	1.96/1.98
5.7-I	C_2/C_{2v}	3.83/4.11	5	3.00/2.92	1.80/1.85
5.7-II	C_s	3.76/4.10	3	2.73/2.61	1.85/1.87
5.7-III	C_1/C_s	3.75/4.10	5	2.86/2.76	1.86/1.88
5.8-I	C_s	3.69/4.07	7/5	3.06/2.88	1.82/1.84
5.8-II	C_1	3.66/4.01	9/7	2.83/2.86	1.91/1.91
5.8-III	C_2/C_s	3.58/3.97	9/9	2.79/2.75	1.94/1.96

TABLE VII: Several properties of neutral nickel oxide clusters:

Signature <i>n.m</i> -isomer	neutral						
	Sym	$E_b(n, m)$	I_p	E_a	μ	D(Ni-Ni)	D(Ni-O)
6.1-I	C_s	2.88	6.33	1.39	6	2.45	1.95
6.1-II	C_{3v}	2.87	6.33	1.68	6	2.46	1.92
6.1-III	C_{2v}	2.86	6.60	1.85	6	2.43	1.84
6.2-I	C_{2v}	3.25	6.78	1.83	8	2.51	1.92
6.2-II	D_{3d}	3.18	6.64	1.72	4	2.48	1.90
6.2-III	C_{2v}	3.21	6.98	2.03	6	2.52	1.92
6.3-I	C_{3v}	3.56	7.15	3.15	8	2.52	1.92
6.3-II	C_s	3.44	6.83	2.05	6	2.53	1.93
6.3-III	C_{2v}	3.44	7.36	2.34	8	2.54	1.83
6.4-I	T_d	3.80	7.45	2.37	8	2.56	1.92
6.4-II	C_1	3.64	7.11	3.95	4	2.38	1.89
6.4-III	D_{2h}	3.63	7.07	2.35	6	2.62	1.92
6.5-I	C_1	3.80	7.40	3.90	10	2.83	1.88
6.5-II	C_1	3.78	7.24	2.74	10	1.73	1.92
6.5-III	C_{3v}	3.81	7.61	2.59	4	2.59	1.92
6.6-I	D_{3h}	3.87	7.21	2.89	2	2.58	1.93
6.6-II	C_s	3.86	7.19	2.92	2	2.79	1.92
6.6-III	C_1	3.82	7.80	3.90	2	3.09	1.75
6.7-I	C_{3v}	3.92	7.99	3.52	4	2.59	1.94
6.7-II	C_s	3.90	8.26	3.31	4	2.61	1.93
6.7-III	C_s	3.83	8.38	3.60	10	2.77	1.88
6.8-I	O_h	3.98	8.84	3.91	4	2.59	1.94
6.8-II	D_{4h}	3.82	8.76	4.25	6	2.64	1.83
6.9-I	C_{4v}	3.88	9.01	4.35	8	2.68	1.95

TABLE VIII: Several properties of cationic and anionic nickel oxide clusters:

Signature <i>n.m</i> -isomer	Sym	$E_b(n, m)$	μ	cation/anion	
				D(Ni-Ni)	D(Ni-O)
6.1-I	C_s	3.07/3.05	7/5	2.52/2.45	1.92/1.97
6.1-II	C_{2v}/C_{3v}	3.07/3.10	7	2.65/2.43	1.91/1.94
6.1-III	C_{2v}	3.02/3.06	7	2.45/2.42	1.82/1.86
6.2-I	C_{2v}	3.36/3.46	7	2.51/2.49	1.90/1.93
6.2-II	C_2/C_1	3.32/3.38	7/5	2.51/2.45	1.89/1.92
6.2-III	C_{2v}	3.30/3.45	5/7	2.47/2.45	1.83/1.84
6.3-I	C_s/C_{3v}	3.62/3.78	9/7	2.69/2.51	1.90/1.92
6.3-II	C	3.54/3.65	7	2.67/2.52	1.91/1.95
6.3-III	C_{2v}	3.48/3.69	7	2.56/2.52	1.80/1.83
6.4-I	T_d	3.83/4.02	5/7	2.59/2.54	1.89/1.92
6.4-II	$C_1/ -$	3.70/ -	9/-	2.71/ -	1.89/ -
6.4-III	D_{4h}/D_{2h}	3.70/3.86	7/5	2.71/2.55	1.89/1.93
6.5-I	C_1/D_{3h}	3.83/4.14	11/9	2.53/2.51	1.88/1.87
6.5-II	C_1	3.82/4.02	11/9	2.81/2.65	1.92/1.94
6.5-III	C_{3v}/C_1	3.82/4.03	5/7	2.68/2.58	1.92/2.01
6.6-I	C_s/C_{3v}	3.91/4.10	1/7	3.03/2.72	1.94/1.95
6.6-II	C_1/D_{2h}	3.91/4.10	3/11	2.77/2.60	1.91/2.01
6.6-III	D_{6h}/C_1	3.81/4.07	1/11	3.33/2.92	1.75/1.79
6.7-I	C_{3v}	3.90/4.18	7/3	2.67/2.58	1.94/1.94
6.7-II	C_s	3.86/4.15	5	2.67/2.67	1.92/1.94
6.7-III	C_s/C_1	3.78/4.10	11/9	2.83/2.74	1.87/1.89
6.8-I	O_h	3.90/4.25	5/3	2.62/2.58	1.94/1.95
6.8-II	D_{4h}	3.74/4.11	7/9	2.75/2.75	1.83/1.84
6.9-I	C_{4v}	3.79/4.16	9/7	2.76/2.66	1.95/1.95

TABLE IX: Several properties of neutral nickel oxide clusters:

Signature <i>n.m</i> -isomer	neutral						
	Sym	$E_b(n, m)$	I_p	E_a	μ	D(Ni-Ni)	D(Ni-O)
7.1-I	C_s	2.96	6.31	1.66	8	2.47	1.92
7.1-II	C_s	2.93	6.12	1.81	8	2.48	1.92
7.1-III	C_s	2.91	6.11	1.68	8	2.45	1.94
7.2-I	C_s	3.29	6.77	1.99	8	2.49	1.92
7.2-II	C_2	3.25	6.56	1.98	8	2.45	1.93
7.2-III	C_s	3.21	6.56	1.84	6	2.48	1.91
7.3-I	C_{3v}	3.58	7.95	2.13	8	2.50	1.92
7.3-II	C_{3v}	3.57	6.77	1.88	8	2.52	1.92
7.3-III	C_1	3.41	6.61	3.00	8	2.56	1.94
7.4-I	C_s	3.71	7.13	2.44	8	2.54	1.91
7.4-II	C_s	3.71	7.21	2.61	8	2.54	1.89
7.4-III	C_{3v}	3.58	6.53	2.53	4	2.53	1.93
7.5-I	C_s	3.87	7.52	3.06	10	2.54	1.90
7.5-II	C_s	3.72	6.86	2.60	8	2.66	1.80
7.5-III	C_{2v}	3.74	7.30	3.84	10	2.66	1.93
7.6-I	C_{3v}	3.89	7.43	3.40	12	2.65	1.88
7.6-II	C_{3v}	3.86	7.23	2.99	12	2.66	1.94
7.6-III	C_1	3.86	7.50	3.44	10	2.54	1.90
7.7-I	C_{3v}	3.93	7.55	2.99	2	2.82	1.88
7.7-II	C_s	3.89	7.60	3.00	6	2.72	1.94
7.7-III	C_{3v}	3.86	7.84	3.34	4	2.53	1.95
7.8-I	C_s	3.96	7.81	3.32	6	2.82	1.84
7.8-II	C_s	3.95	7.94	3.24	4	2.83	1.88
7.8-III	C_s	3.94	7.98	3.53	2	2.85	1.88
7.9-I	C_s	3.98	8.24	3.65	4	2.88	1.90
7.9-II	C_{3v}	3.96	8.26	3.63	4	2.85	1.90
7.10-I	C_{3v}	4.01	8.43	3.87	6	2.91	1.91

TABLE X: Several properties of cationic and anionic nickel oxide clusters:

Signature <i>n.m</i> -isomer	Sym	$E_b(n, m)$	μ	cation/anion	
				D(Ni-Ni)	D(Ni-O)
7.1-I	C_s	3.14/3.15	7	2.50/2.44	1.90/1.93
7.1-II	C_s/C_1	3.13/3.14	7	2.49/2.47	1.91/1.95
7.1-III	C_1/C_s	3.11/3.10	7	2.58/2.45	1.90/1.93
7.2-I	C_1/C_s	3.40/3.50	9/7	2.52/2.47	1.91/1.92
7.2-II	C_2	3.38/3.45	7	2.51/2.48	1.91/1.95
7.2-III	C_s	3.34/3.40	7/5	2.52/2.47	1.90/1.93
7.3-I	C_s/C_{3v}	3.65/3.78	9/7	2.59/2.49	1.90/1.93
7.3-II	C_s/C_{3v}	3.57/3.65	9/7	2.66/2.52	1.90/1.93
7.3-III	C_1	3.52/3.70	9/7	2.62/2.69	1.93/1.94
7.4-I	C_s	3.76/3.92	9/7	2.61/2.53	1.90/1.93
7.4-II	C_1/C_s	3.75/3.93	9/7	2.67/2.55	1.88/1.90
7.4-III	C_{3v}	3.69/3.80	11/9	2.79/2.54	1.94/1.97
7.5-I	C_s/C_{2v}	3.89/4.12	11/9	2.62/2.53	1.88/1.91
7.5-II	C_s	3.79/3.93	9/7	2.73/2.66	1.92/1.94
7.5-III	C_s/C_{2v}	3.77/4.05	11/9	2.74/2.68	1.92/1.97
7.6-I	C_{3v}/C_s	3.91/4.14	5/11	2.79/2.63	1.84/1.89
7.6-II	C_1/C_{3v}	3.90/4.08	13/11	2.85/2.60	1.94/1.97
7.6-III	C_s/C_1	3.87/4.11	11/9	2.79/2.86	1.89/1.92
7.7-I	C_{3v}	3.94/4.14	1/5	2.84/2.78	1.88/1.92
7.7-II	C_s	3.91/4.10	11/7	2.79/2.68	1.93/1.95
7.7-III	C_{3v}	3.85/4.09	11/3	2.57/2.52	1.92/1.95
7.8-I	C_s	3.95/4.17	7/5	2.85/2.58	1.93/1.93
7.8-II	C_1/C_s	3.94/4.16	5/9	2.89/2.82	1.88/1.91
7.8-III	C_1/C_s	3.93/4.17	3	3.05/2.80	1.87/1.89
7.9-I	C_s	3.95/4.20	3/5	2.92/2.82	1.89/1.91
7.9-II	C_{3v}	3.93/4.18	11/5	2.95/2.82	1.91/1.91
7.10-I	C_{3v}	3.97/4.23	5	2.91/2.88	1.90/1.92

TABLE XI: Several properties of neutral nickel oxide clusters:

Signature <i>n.m</i> -isomer	neutral						
	Sym	$E_b(n, m)$	I_p	E_a	μ	D(Ni-Ni)	D(Ni-O)
8.1-I	C_s	3.03	6.32	1.76	8	2.45	1.92
8.1-II	C_1	3.00	6.30	1.70	8	2.51	1.93
8.1-III	C_s	2.99	6.35	1.88	8	2.53	1.90
8.2-I	C_{2v}	3.35	6.69	1.94	8	2.46	1.92
8.2-II	C_s	3.27	6.56	1.91	8	2.56	1.91
8.2-III	C_s	3.24	6.81	2.38	10	2.54	1.82
8.3-I	C_1	3.50	6.57	2.23	8	2.54	1.91
8.3-II	C_s	3.47	6.66	2.28	10	2.50	1.90
8.3-III	C_s	3.48	6.83	2.38	8	2.56	1.89
8.4-I	C_{2v}	3.67	7.15	2.62	10	2.53	1.91
8.4-II	S_2	3.64	6.88	2.32	8	2.58	1.90
8.4-III	C_1	3.64	7.06	2.69	10	2.51	1.90
8.5-I	C_{2v}	3.84	7.33	2.61	10	2.53	1.94
8.5-II	C_1	3.73	5.98	2.86	10	2.62	1.90
8.5-III	C_{2v}	3.70	7.09	2.78	12	2.60	2.09
8.6-I	C_{4v}	3.87	9.41	2.83	12	2.56	1.98
8.6-II	C_1	3.88	8.18	3.11	4	2.65	1.91
8.6-III	C_{2v}	3.72	7.39	2.92	4	2.52	1.94
8.7-I	C_1	3.94	7.33	3.26	10	2.70	1.91
8.7-II	C_s	3.92	7.27	2.96	12	2.77	1.93
8.7-III	C_1	3.92	7.46	2.93	8	2.80	1.94
8.8-I	C_1	3.97	7.40	3.20	4	2.71	1.83
8.8-II	C_s	3.96	7.30	3.40	8	2.75	1.92
8.9-I	C_1	3.97	7.06	3.72	8	2.78	1.92
8.9-II	C_1	4.00	7.82	3.35	8	2.93	1.93
8.9-III	C_1	3.97	7.39	3.66	12	2.78	1.94
8.10-I	C_1	4.02	7.92	3.99	2	2.80	1.85
8.10-II	C_1	4.00	8.07	3.93	4	2.60	1.91

TABLE XII: Several properties of cationic and anionic nickel oxide clusters:

Signature <i>n.m</i> -isomer	Sym	$E_b(n, m)$	μ	cation/anion	
				D(Ni-Ni)	D(Ni-O)
8.1-I	C_s	3.18/3.21	9/7	2.48/2.46	1.91/1.93
8.1-II	C_1	3.15/3.17	9/7	2.54/2.51	1.92/1.94
8.1-III	C_s	3.15/3.19	9	2.52/2.53	1.90/1.94
8.2-I	C_{2v}	3.45/3.53	9/7	2.52/2.46	1.91/1.92
8.2-II	C_s	3.39/3.45	9/7	2.59/2.55	1.91/1.92
8.2-III	C_s	3.33/3.46	9	2.57/2.51	1.82/1.84
8.3-I	C_s/C_1	3.60/3.69	9/7	2.45/2.39	1.91/1.93
8.3-II	C_s	3.56/3.66	11/9	2.55/2.55	1.90/1.92
8.3-III	C_s	3.56/3.69	9/7	2.56/2.52	1.88/1.89
8.4-I	C_1/C_{2v}	3.72/3.88	11/9	2.61/2.51	1.90/1.92
8.4-II	C_1/s_4	3.70/3.82	9/7	2.63/2.57	1.89/1.91
8.4-III	C_s/C_1	3.69/3.85	11/9	2.62/2.60	1.89/1.91
8.5-I	C_{2v}	3.87/4.03	11/9	2.55/2.50	1.93/1.96
8.5-II	C_1	3.87/3.94	11/9	2.65/2.63	1.88/1.92
8.5-III	C_{2v}	3.75/3.91	13/11	2.63/2.64	1.96/1.98
8.6-I	C_{4v}	3.90/4.06	11	2.65/2.55	1.96/1.97
8.6-II	C_{2v}/C_1	3.85/4.10	7	2.68/2.80	1.90/1.89
8.6-III	C_{2v}	3.75/3.92	5/3	2.57/2.51	1.93/1.95
8.7-I	C_1	3.96/4.14	9	2.80/2.69	1.91/1.92
8.7-II	C_1/C_s	3.95/4.10	9/11	2.74/2.67	1.92/1.95
8.7-III	C_1	3.93/4.10	11/9	2.87/2.74	1.90/1.97
8.8-I	C_1	3.99/4.16	7	2.75/2.73	1.91/1.93
8.8-II	C_s/C_{4v}	3.98/4.15	5/7	2.76/2.78	1.92/1.93
8.9-I	C_1	4.00/4.18	7	2.80/2.66	1.86/1.93
8.9-II	C_1	3.99/4.20	9/7	2.75/2.89	1.93/1.94
8.9-III	C_s/C_1	3.98/4.18	11/7	2.81/2.77	1.87/1.87
8.10-I	C_2	4.01/4.24	9/7	2.81/2.78	1.91/1.92
8.10-II	C_1	3.98/4.21	9/7	2.65/2.54	1.93/1.93